High-tolerance antiblockade SWAP gates using optimal pulse drivings

Wan-Xia Li,[1] Jin-Lei Wu,[2] Shi-Lei Su,[2] and Jing Qian[1,3,*]

[1]*State Key Laboratory of Precision Spectroscopy, Department of Physics, School of Physics and Electronic Science, East China Normal University, Shanghai 200062, China*

[2]*School of Physics, Zhengzhou University, Zhengzhou 450001, China*

[3]*Shanghai Branch, Hefei National Laboratory, Shanghai 201315, China*

(Received 4 September 2023; accepted 11 December 2023; published 8 January 2024)

Position error is treated as the leading obstacle that prevents Rydberg antiblockade gates from being experimentally realizable, because of the inevitable fluctuations in the relative motion between two atoms, invalidating the antiblockade condition. In this work we report progress towards a high-tolerance antiblockade-based Rydberg SWAP gate enabled by the use of a modified antiblockade condition combined with carefully optimized laser pulses. Depending on the optimization of diverse pulse shapes, our protocol shows that the amount of time spent in the double Rydberg state can be shortened by more than 70% with respect to the case using the perfect antiblockade condition, which significantly reduces this position error. Moreover, we benchmark the robustness of the gate by taking into account the technical noises, such as the Doppler dephasing due to atomic thermal motion, the fluctuations in laser intensity and laser phase, and the intensity inhomogeneity. Compared to other existing antiblockade-gate schemes, we are able to maintain a predicted gate fidelity above 0.91 after a very conservative estimation of various experimental imperfections, especially considered for a realistic interaction deviation of $\delta V/V \approx 5.92\%$ at $T \sim 20$ μK. Our work creates an opportunity for the experimental demonstration of Rydberg antiblockade gates in the near future.

DOI: 10.1103/PhysRevA.109.012608

I. INTRODUCTION

Implementation of Rydberg antiblockade gates is one of the current mainstream protocols towards fast and robust neutral-atom quantum computation [1–6], as the traditional Rydberg antiblockade regime with enhanced dissipative dynamics can lead to the preparation of high-fidelity steady entanglement in versatile systems [7–17]. Beyond applications in quantum entanglement, constructing a quantum logic gate via the antiblockade effect [18–20] is more straightforward because the simultaneous multiatom excitation establishes an effective model which exactly avoids the occupancy of lossy singly-excited Rydberg states. Despite these significant advances, however, owing to the leading participation of multiatom excited states, such antiblockade gates are found to be extremely sensitive to the relative position fluctuations between two atoms [21–24] as well as to atomic decays [25], which so far has inherently precluded its experimental validation.

Based on the antiblockade mechanism, some prior studies of, e.g., control-phase gates [26] presented a gate infidelity far larger than 0.15 for an interaction deviation of $\delta V/V \approx 5.0\%$. More recently, Wu *et al.* [27] demonstrated two-atom SWAP gates with an infidelity of approximately 0.03 when the position deviation in the interatomic distance is only approximately 3.0 nm, resulting from using a deep cooling of ground-state qubits [28–30] or sufficiently deep traps [31]. Therefore, although the antiblockade mechanism can lead to high-fidelity Rydberg gates in theory, their implementation in experiment thus far remains unachievable. A realistic position-error-tolerant scheme is urgently needed.

In this paper we present a practical scheme to realize the antiblockade SWAP gates with greatly improved tolerance, especially to the significant fluctuations in interatomic interactions. We optimize different laser pulse shapes for minimizing the time spent in the double Rydberg state, so as to decrease the sensitivity of the gate to the interatomic distance deviation. It is observable that, accompanied by a modified antiblockade condition $V = \Delta_1 + \Delta_2 + q$, which contains a nonzero factor q to loosen the antiblockade constraint, the occupancy of the double Rydberg state can be strongly suppressed for an arbitrary pulse shape [32]. Recall that in a perfect antiblockade-gate scheme where the interaction energy is perfectly compensated by the detunings between the driving field and atomic transition, i.e., $V = \Delta_1 + \Delta_2$, it is challenging to construct quantum gate operations since some unwanted ac Stark shift terms would emerge in the effective Hamiltonian [see Eq. (6)], although the excitation of a single atom has been eliminated by off-resonant couplings. We find that the ideal two-qubit SWAP gates, in the absence of any position deviation, have an average fidelity of $\mathcal{F} \sim 0.9997$. In addition, even taking into account other technical imperfections, a more conservative estimation of $\mathcal{F} \geqslant 0.9140$ arises for a typical 1.0-μs gate duration, which is mainly caused by the position error approximately equal to 0.0752 considered for an atomic temperature of $T \sim 20$ μK (equivalently $\delta V/V \approx 5.92\%$). We also verify that the characteristic timescale for

*jqian1982@gmail.com

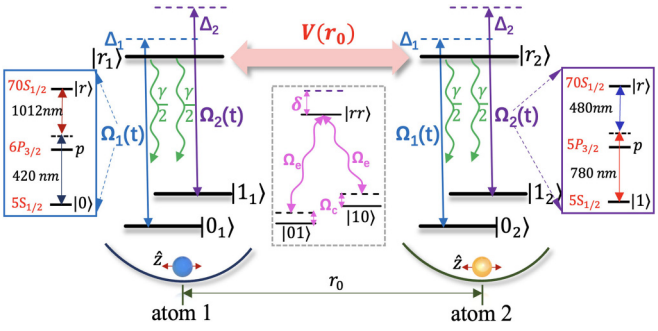

FIG. 1. Level structure of two-qubit Rydberg SWAP gates based on modified antiblockade. The central inset gives an effective swapping model formed by an off-resonance Raman-like transition on two targeted states $|01\rangle$ and $|10\rangle$ mediated by $|rr\rangle$. The atomic qubits are defined as hyperfine clock qubits encoded in ground energy levels $|0_{1,2}\rangle = |5S_{1/2}, F = 1, m_F = 0\rangle$ and $|1_{1,2}\rangle = |5S_{1/2}, F = 2, m_F = 0\rangle$. Here $|r_{1,2}\rangle = |70S_{1/2}\rangle$ is the Rydberg state considered for a ^{87}Rb experiment [40]. The vdW dispersion coefficient for the doubly-excited state $|70S_{1/2}; 70S_{1/2}\rangle$ is $C_6/2\pi = 862.69$ GHz μm^6 [41], leading to the nonfluctuating Rydberg interaction strength $V/2\pi \approx 70.49$ MHz at a fixed distance $r_0 = 4.8$ μm. The Rydberg decay rate is $\gamma = 2\pi/\tau$, with τ (≈400 μs) the lifetime of Rydberg states. See the text for more details.

the gate is determined by the maximal Rabi frequency of the driving lasers. When their maxima are restricted to be smaller than $2\pi \times 50$ MHz cooperating with the optimization for the gate duration, a faster (approximately 0.1177 μs) antiblockade SWAP gate is achievable which contains a higher tolerance to the position error due to the less time spent in the Rydberg state (see Appendix B for an extended study).

Our implementation building on the earlier proposal of antiblockade gates [27] additionally adopts optimal time-dependent pulse drivings, which not only avoids the combination of a series of elementary gates [33] and realizes the nontrivial SWAP gate within one-step implementation, but also greatly improves the antiblockade-gate robustness against fundamental position fluctuations between two trapped atoms. The SWAP gate is important with extensive applications in, e.g., quantum entanglement swapping [34–36] and quantum repeaters [37–39]. In contrast to other existing proposals, the parameters we set to realize the gate are all extracted from careful optimization which can provide an opportunity to decrease the leading obstacle i.e., the position error that mainly restricts the antiblockade gate fidelity.

II. THEORETICAL STRATEGY

In this work we propose a two-qubit SWAP gate with high position-error tolerance based on a modified antiblockade condition. As illustrated in Fig. 1, two identical neutral atoms, individually trapped in two optical tweezers, have hyperfine ground states $|0\rangle$ and $|1\rangle$ and Rydberg state $|r\rangle$. When atoms are simultaneously excited they interact via the Rydberg-Rydberg interaction. Here the interaction strength is quantified by $V = C_6/r_0^6$, denoting a van der Waals (vdW)–type interaction. During the laser-based operation the excitation $|0\rangle \to |r\rangle$ in each atom is accomplished by a two-photon process with effective Rabi frequency $\Omega_1(t)$ and two-photon detuning Δ_1. Similarly, the other transition $|1\rangle \to |r\rangle$ is accomplished by $\Omega_2(t)$ and Δ_2. Such two-photon processes are usually mediated via different low-lying p states (Fig. 1, insets), which have been adiabatically eliminated due to the large intermediate detunings for p states [42]. In addition, we assume state $|r\rangle$ decays to $|0\rangle$ and $|1\rangle$ with rate γ and equal branching ratios. To be more realistic we introduce a leakage state $|\alpha\rangle$ (not shown in Fig. 1) for each atom outside the qubit basis $\{|0\rangle, |1\rangle\}$. Here we restrict the analysis to the case of $\eta_{r\to 0\,(1)} = \frac{1}{2}$ and $\eta_{r\to\alpha} = 0$, which provides an ideal estimation of the gate fidelity.

With the rotating-wave approximation, the total Hamiltonian for this system can be described by ($\hbar = 1$ hereafter)

$$\hat{\mathcal{H}} = \hat{\mathcal{H}}_1 \otimes \hat{\mathcal{I}}_2 + \hat{\mathcal{I}}_1 \otimes \hat{\mathcal{H}}_2 + \hat{V}_{rr}, \tag{1}$$

where

$$\hat{\mathcal{H}}_j = \Omega_1 e^{-i\Delta_1 t}|0\rangle_j\langle r| + \Omega_2 e^{-i\Delta_2 t}|1\rangle_j\langle r| + \text{H.c.} \tag{2}$$

accounts for the jth atom coupling to the driving lasers and

$$\hat{V}_{rr} = V|rr\rangle\langle rr| \tag{3}$$

is the interaction between the Rydberg states. Here $j \in (1, 2)$ and $\hat{\mathcal{I}}_j$ denotes the identity matrix.

While deriving the effective form of $\hat{\mathcal{H}}$ through the second-order perturbation calculation we apply two parameter conditions. One is $|\Delta_1| \gg \Omega_1^{\max}$ and $|\Delta_2| \gg \Omega_2^{\max}$, which aims at canceling the population on singly-excited Rydberg states by off-resonant couplings. The resulting single-excitation terms are all decoupled to the initial states and can be discarded [see Eq. (A11)]. The other is $V = \Delta_1 + \Delta_2 + q$, representing a modified antiblockade condition in which the presence of the factor q is crucial for suppressing unwanted population on state $|rr\rangle$. Note that $q = 0$ reduces to the case of perfect antiblockade in which the double Rydberg state $|rr\rangle$ can obtain a facilitated excitation because of the perfect compensation between V and $\Delta_1 + \Delta_2$ [43]. However, when $q \neq 0$, known as the modified antiblockade, one can modify the antiblockade regime by changing the Stark shift terms of $|rr\rangle$ and therefore shorten the time spent on it [44].

After rotating with respect to the operator $\hat{U} = e^{-i(\Delta_1+\Delta_2)t|rr\rangle\langle rr|}$, the effective formula of $\hat{\mathcal{H}}$ can be separately written as

$$\hat{\mathcal{H}}_{00,\text{eff}} = \frac{2\Omega_1^2}{\Delta_1}|00\rangle\langle 00|, \tag{4}$$

$$\hat{\mathcal{H}}_{11,\text{eff}} = \frac{2\Omega_2^2}{\Delta_2}|11\rangle\langle 11| \tag{5}$$

for initial states $|00\rangle$ and $|11\rangle$, respectively, and

$$\begin{aligned}\hat{\mathcal{H}}_{01,\text{eff}} = {} & \Omega_e(|rr\rangle\langle 01| + |rr\rangle\langle 10|) + \text{H.c.} \\ & + \Omega_c(|01\rangle\langle 01| + |10\rangle\langle 10|) + \delta|rr\rangle\langle rr|\end{aligned} \tag{6}$$

for initial states $|01\rangle$, where

$$\begin{aligned}\Omega_e &= \frac{\Omega_1\Omega_2}{\Delta_1} + \frac{\Omega_1\Omega_2}{\Delta_2}, \quad \Omega_c = \frac{\Omega_1^2}{\Delta_1} + \frac{\Omega_2^2}{\Delta_2}, \\ \delta &= \frac{2\Omega_2^2}{\Delta_1} + \frac{2\Omega_1^2}{\Delta_2} + q\end{aligned} \tag{7}$$

denote the effective couplings, the ac Stark shift with respect to $|01\rangle$ and $|10\rangle$, and the effective detuning (including ac Stark shifts) to $|rr\rangle$, respectively. From Eqs. (4)–(6) we see that states $|00\rangle$ and $|11\rangle$ are dark to all gate pulses as expected, whereas if the initially considered states are $|01\rangle$ or $|10\rangle$, the system will reduce to an effective three-level swapping model. Since states $|10\rangle$ and $|01\rangle$ exhibit equivalent dynamics in this symmetric setup, $\hat{\mathcal{H}}_{10,\text{eff}} = \hat{\mathcal{H}}_{01,\text{eff}}$. More details about the derivation of Eqs. (4)–(6) can be found in Appendix A.

From $\hat{\mathcal{H}}_{01,\text{eff}}$ we find an effective three-level system for states $|01\rangle$ and $|10\rangle$ is off-resonantly coupled to $|rr\rangle$ (Fig. 1, inset). Thus one can expect that the combined action of all quantities including Ω_e, Ω_c, and δ will achieve a perfect state swapping by obeying

$$|01\rangle \rightleftarrows |rr\rangle \rightleftarrows |10\rangle. \tag{8}$$

However, the simultaneous participation of the Rydberg excitation state $|rr\rangle$ in this process will no doubt suffer from a serious position error, mainly caused by the significant deviation of the interatomic interaction δV(with respect to the nonfluctuating strength V) between individually trapped atoms that breaks the antiblockade condition [45]. Fortunately, the effective detuning δ to state $|rr\rangle$ contains a factor q which provides a more flexible adjustment to the original ac Stark shift term $\frac{2\Omega_2^2}{\Delta_1} + \frac{2\Omega_1^2}{\Delta_2}$ on $|rr\rangle$. We show a positive q that modifies the ac Stark shift which can make state $|rr\rangle$ far-off-resonance so as to reduce the population on it [46]. Therefore, our protocol can exhibit a higher tolerance against significant interaction fluctuations arising from, e.g., the thermal motion of atoms in the inhomogeneous coupling field [47] or laser intensity noise [48].

III. GATE IMPLEMENTATION WITH OPTIMAL PULSES

Now we show that the two-qubit SWAP gates can be realized for diverse pulse shapes $\Omega_1(t)$ and $\Omega_2(t)$. We perform global numerical optimization for all pulse parameters and laser detunings by using the genetic algorithm as in our prior work [49], which aims at maximizing the ideal gate fidelity. Note that all stochastic deviations arising from technical imperfections are excluded in the perfect optimization case, and the gate robustness against main error sources will be analyzed after the perfect optimization (Secs. IV and V). A different choice of optimization algorithm combined with a careful consideration of the gate robustness to some type of errors [50] is left for future work.

To fully understand the population dynamics, we numerically solve the two-atom master equation in the Lindblad form [51]

$$\dot{\rho} = -i[\hat{\mathcal{H}}, \hat{\rho}] + \frac{1}{2}\sum_{j=1}^{6}[2\hat{\mathcal{L}}_j\hat{\rho}\hat{\mathcal{L}}_j^\dagger - (\hat{\mathcal{L}}_j^\dagger\hat{\mathcal{L}}_j\hat{\rho} + \hat{\rho}\hat{\mathcal{L}}_j^\dagger\hat{\mathcal{L}}_j)], \tag{9}$$

where the single-atom decay operator $\hat{\mathcal{L}}_j$ expressed in the basis $\{|0\rangle, |1\rangle, |r\rangle, |\alpha\rangle\}$ ($|\alpha\rangle$ is a leakage state) is given by

$$\begin{aligned}
\hat{\mathcal{L}}_1 &= \sqrt{\eta_{r\to0}\gamma}|0\rangle_1\langle r|, \quad \hat{\mathcal{L}}_2 = \sqrt{\eta_{r\to0}\gamma}|0\rangle_2\langle r|,\\
\hat{\mathcal{L}}_3 &= \sqrt{\eta_{r\to1}\gamma}|1\rangle_1\langle r|, \quad \hat{\mathcal{L}}_4 = \sqrt{\eta_{r\to1}\gamma}|1\rangle_2\langle r|,\\
\hat{\mathcal{L}}_5 &= \sqrt{\eta_{r\to\alpha}\gamma}|\alpha\rangle_1\langle r|, \quad \hat{\mathcal{L}}_6 = \sqrt{\eta_{r\to\alpha}\gamma}|\alpha\rangle_2\langle r|,
\end{aligned} \tag{10}$$

representing all Rydberg-state scattering channels, with $|r\rangle \to |\alpha\rangle$ denoting the leakage out of the qubit manifold to other m_F states. In the calculation we have assumed that state $|r\rangle$ decays to the ground-state manifold $|0\rangle$ and $|1\rangle$ uniformly with equal probability $\eta_{r\to0} = \eta_{r\to1} = \frac{1}{2}$, and $\eta_{r\to\alpha} = 0$. An extended calculation based on a realistic eight-ground-state manifold will be discussed in Appendix B. Numerical solutions of Eq. (9) can be directly used to extract the average gate fidelity in the perfect optimization case over four input states $\{|00\rangle, |01\rangle, |10\rangle, |11\rangle\}$ as

$$\mathcal{F} = \tfrac{1}{4}\text{Tr}\sqrt{\sqrt{U}\rho(t = T_g)\sqrt{U}}, \tag{11}$$

with 4 the number of input states, U the ideal transfer matrix for the two-qubit SWAP operation, and $\rho(t)$ the practical density matrix measured at $t = T_g$ (gate duration). For any input state one can obtain the full population dynamics of an arbitrary intermediate state along with the above master equation (9).

To obtain an antiblockade SWAP gate with high tolerance, the leading step is to find optimal pulse shapes with an appropriate q, where the time spent in the Rydberg level can be minimized, especially in the double Rydberg state $|rr\rangle$. For comparison, we demonstrate the gate using different pulse shapes as done in [52]. The characteristic timescale T_g for the gate is constrained by the maximal Rabi frequency $(\Omega_1^{\max}, \Omega_2^{\max})$ of the driving lasers that should meet the swapping circles. Since here we focus on comparing the gate performance under different pulse shapes, T_g is fixed to 1.0 μs for simplicity. This choice restricts the maximal strength of Rabi frequencies to be approximately $2\pi \times 10$ MHz. A larger two-photon Rabi frequency (approximately $2\pi \times 50$ MHz) can further decrease the T_g value to the level of approximately 0.1 μs, which is promising for the realization of a faster gate with improved robustness. The relationship between T_g and $\Omega_{1,2}^{\max}$ is numerically confirmed by an extended study involving an optimal T_g (Appendix B). In order to show the significance of q, we seek optimal pulse parameters individually for two cases, $q = 0$ and $q \neq 0$, which are summarized in Table I. The corresponding full population dynamics are comparably displayed in Fig. 2.

First we demonstrate the gate with two optimal isosceles-triangle-shaped pulses via assuming, for case i,

$$\Omega_j(t) = \begin{cases} \Omega_j^{\max} & \text{for } t = \frac{T_g}{2} \\ 0 & \text{for } t = 0, T_g. \end{cases}$$

This triangular pulse shape only involves one parameter $\Omega_j^{\max}$ to be optimized in addition to Δ_1 and q. As can be seen from Figs. 2(a 1)–2(e 1) and 2(a 4)–2(e 4), although the peak Rabi frequencies $\Omega_1^{\max}$ and $\Omega_2^{\max}$ are comparable to each other, the case in Figs. 2(a 4)–2(e 4) with $q \neq 0$ clearly causes a large energy shift for the effective detuning $\delta(t)$ [green dashed line in Fig. 2(b 4)] which enables a big reduction in the time spent in the double Rydberg state. We verify this by calculating the duration in state $|rr\rangle$ for input $|01\rangle$ and find that, in Fig. 2(e 1) with $q = 0$, the time spent defined by a time integration is $T_{rr} = \int_0^{T_g}\rho_{rr}(t)dt \approx 0.0926$ μs, while this value can reduce to $T_{rr} \approx 0.0248$ μs in the case of Fig. 2(e 4) where $q/2\pi = 4.668$ MHz (optimal), which shortens the time spent in the double Rydberg state by 73.2%. Such a large reduction

TABLE I. Optimal pulse parameters and optimal laser detunings with different pulse shapes for $q = 0$ and $q \neq 0$: case i, isosceles triangle; case ii, Gaussian; and case iii, composite. Parameters such as $\Omega_j^{\max}$, Ω_{0j}, Ω_{1j}, Ω_{2j}, Δ_1, and q are all in units of $2\pi \times$ MHz and ω_j is in unit of μs. In any case the antiblockade condition $V = \Delta_1 + \Delta_2 + q$ is always satisfied and $V = 2\pi \times 70.49$ MHz is treated as the ideal (nonfluctuating) interaction strength between two atoms at a fixed distance r_0. The gate duration $T_g = 1.0$ μs is unvaried. The ideal gate fidelity $\mathcal{F}$ calculated in the absence of any technical imperfection is given in the last column. The Rydberg decay error intrinsically caused by the limited lifetime of Rydberg levels can be roughly estimated as $1 - \mathcal{F}$.

		Case i		
q	$\Omega_1^{\max}$	$\Omega_2^{\max}$	Δ_1	$\mathcal{F}$
0	3.769	10.441	26.642	0.9992
4.668	5.513	10.947	23.090	0.9996
		Case ii		
q	$(\Omega_1^{\max}, \Omega_2^{\max})$	(ω_1, ω_2)	Δ_1	$\mathcal{F}$
0	(3.595,9.219)	(0.279,0.189)	23.924	0.9993
5.037	(5.114,8.948)	(0.257,0.351)	22.110	0.9997
		Case iii		
q	$(\Omega_{01}, \Omega_{11}, \Omega_{21})$	$(\Omega_{02}, \Omega_{12}, \Omega_{22})$	Δ_1	$\mathcal{F}$
0	(1.033, −1.167, 1.334)	(3.100, −2.662, 2.617)	25.194	0.9992
5.090	(1.774, −1.884, 2.036)	(2.558, −2.624, 2.608)	22.532	0.9997

directly provides an improvement in the average gate fidelity yielding $\mathcal{F} = 0.9996$ (recall that $\mathcal{F} = 0.9992$ for $q = 0$) due to the decrease of the Rydberg decay loss in the perfect case. In addition, we illustrate the validity of the effective Hamiltonian (6) by simulating the effective population dynamics of states $|01\rangle$, $|rr\rangle$, and $|10\rangle$ in Figs. 2(e 1) and 2(e 4). The coincidence between the full and effective models is explicit, confirming the accuracy of our perturbation theory [53].

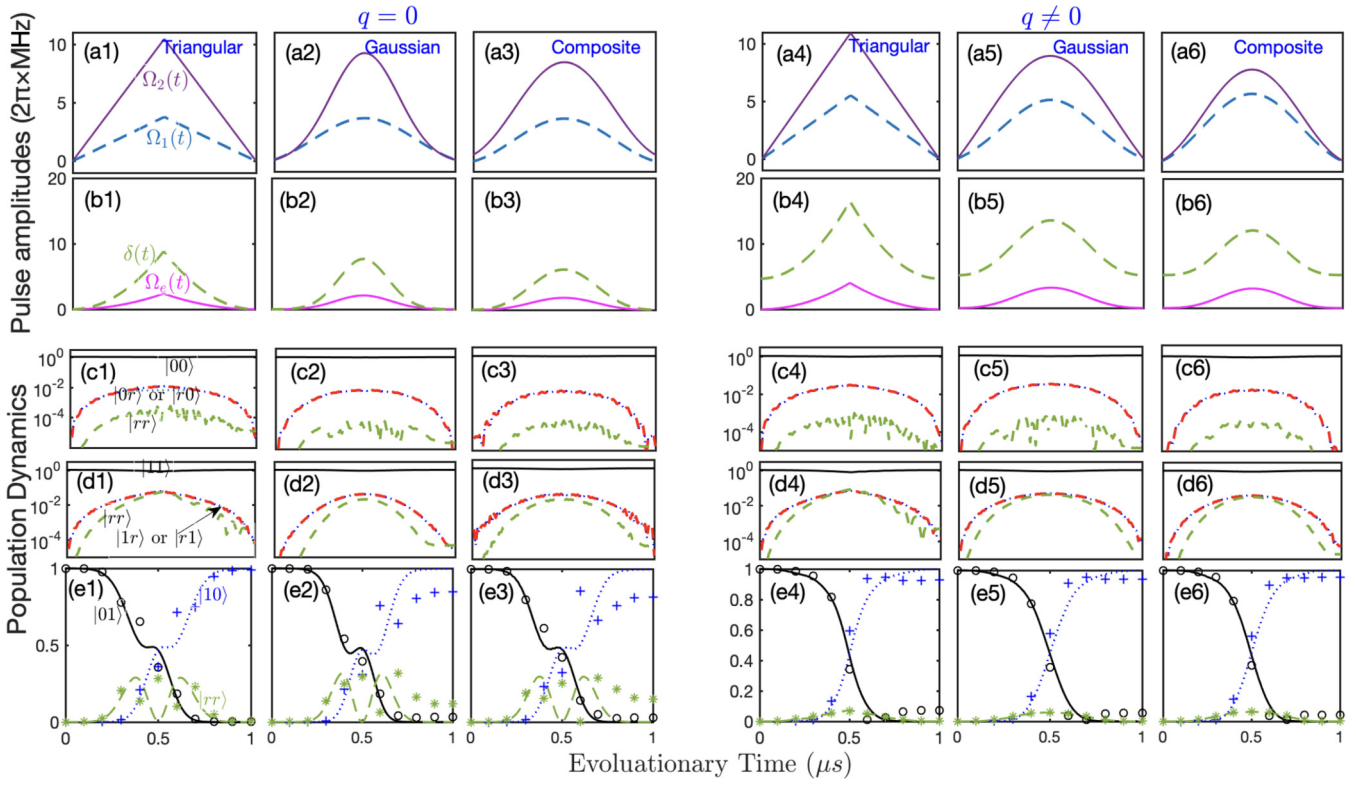

FIG. 2. Realization of two-qubit SWAP gates with different optimal pulse shapes. (a1) and (a4) Optimal isosceles-triangle shaped Rabi frequencies $\Omega_1(t)$ and $\Omega_2(t)$ and (b 1) and (b 4) optimal effective coupling $\Omega_e(t)$ and effective detuning $\delta(t)$ versus the evolutionary time t where $T_g = 1.0$ μs. Here $q = 0$ and $q \neq 0$ stand for the perfect antiblockade and modified antiblockade cases, respectively. The corresponding time-dependent population dynamics based on the original Hamiltonian $\hat{\mathcal{H}}$ for different initial states $\{|00\rangle, |11\rangle, |01\rangle\}$, are displayed in (c 1) and (c 4), (d 1) and (d 4), and (e 1) and (e 4), respectively. In (e 1) and (e 4) the population dynamics of $|01\rangle$ (black circles), $|10\rangle$ (blue pluses), and $|rr\rangle$ (green stars) calculated by the effective Hamiltonian $\hat{\mathcal{H}}_{01,\text{eff}}$ are also comparably displayed. Similar results with optimal Gaussian and composite pulse shapes are given in (a 2)–(e 2) and (a 5)–(e 5) and in (a 3)–(e 3) and (a 6)–(e 6), respectively.

Furthermore, by taking into account the convenience of experimental demonstration, we turn to realize the SWAP gate with smooth-amplitude pulses which contain more variables to be optimized [54]. On the experimental side, the smooth-amplitude gate can help reduce off-resonant coupling to other states which are not included in the idealized model description and provide a finite bandwidth of the laser pulses, reducing the experimental complexity of their fast switching [55]. Here two smooth pulse shapes are considered,

$$\Omega_j(t) = \Omega_j^{\max}\left(\frac{e^{-(t-T_g/2)^2/2\omega_j{}^2} - e^{-(T_g/2)^2/2\omega_j{}^2}}{1 - e^{-(T_g/2)^2/2\omega_j{}^2}}\right) \quad \text{(case ii)},$$

$$\Omega_j(t) = \Omega_{0j} + \Omega_{1j}\cos\left(\frac{2\pi t}{T_g}\right) + \Omega_{2j}\sin\left(\frac{\pi t}{T_g}\right) \quad \text{(case iii)},$$

while keeping Δ_1 and q optimal values (Table I). Also, $\Delta_2 = V - \Delta_1 - q$ is always fulfilled. In particular, in case ii the Gaussian function has been corrected by allowing an exact zero intensity at the start and end of the pulse, which, from an experimental point of view, has a better feasibility [56]. Finally, we present the optimal smooth-amplitude pulses and the population dynamics separately in Figs. 2(a 2)–2(e 2) and 2(a 5)–2(e 5) and in Figs. 2(a 3)–2(e 3) and 2(a 6)–2(e 6), respectively. It is explicit that when $q \neq 0$ the time spent in state $|rr\rangle$ remains at a low level, i.e., $T_{rr} \approx (0.0238, 0.0254)$ μs, resulting in a slightly higher fidelity $\mathcal{F} \approx 0.9997$ than the triangular pulse case. Therefore, although the effective state swapping between $|01\rangle$ and $|10\rangle$ also requires the participation of $|rr\rangle$, its influence has been largely suppressed by applying pulse optimization under the modified antiblockade condition.

So far we have presented the realization of high-fidelity SWAP gates with an arbitrary shape for laser pulses. The key in pulse optimization lies in minimizing the time spent in $|rr\rangle$ by letting $\delta(t)$ be off-resonance in the presence of q, which leads to a direct coupling between $|01\rangle$ and $|10\rangle$. Based on the effective three-level model (Fig. 1), we evaluate the coupling strength by adiabatically eliminating $|rr\rangle$ and find that the effective pulse areas calculated by $\int_0^{T_g} \frac{2\Omega_e(t)^2}{\delta(t)} \approx (3.2600, 3.2318, 3.1946)$ are all close to π for cases i–iii, which strongly confirms the importance of optimizing the pulse area (not pulse shape) in the realization of two-qubit SWAP gates. The resulting gate infidelity mainly caused by the Rydberg decay, denoted by $1 - \mathcal{F} = (3\text{–}4) \times 10^{-4}$, is no doubt very robust to arbitrary pulse shapes.

The participation of the antiblockade condition can facilitate simultaneous excitation from the ground state to the double Rydberg state, strongly suppressing the influence from intermediate singly-excited states, which really gives rise to an efficient one-step implementation of Rydberg gates. Nevertheless, the leading obstacle that limits the robustness of such antiblockade gates becomes its sensitivity in practice to the interaction fluctuations between two Rydberg-state atoms. Typically, they depend on "frozen" Rydberg atomic interactions to fulfill the antiblockade condition [57,58]. In the present work, by minimizing the time spent in $|rr\rangle$ (approximately 0.02 μs) together with the merit of small Rydberg decay errors (approximately 10^{-4}), the gate tolerance to the interaction fluctuations can be largely improved, which is promising for a high-fidelity quantum gate with hotter atoms.

IV. POSITION ERROR TOLERANCE

It is well known that a Rydberg antiblockade gate depends on the leading participation of double Rydberg states and is therefore more sensitive to the fluctuation of interatomic interaction than other gate schemes, such as Rydberg blockade [59,60] or adiabatic passage [61–67]. In reality, this fluctuation in the relative position between two atoms cannot be avoided, especially for two trapped atoms under a finite temperature [68]. That is why the Rydberg antiblockade gates have not been reported by experiments yet. Although, e.g., placing two atoms a long distance apart [69,70] or lowering the atomic temperature [71] can reduce the position error, the robustness of antiblockade gates is still unsatisfactory.

In this section, in order to explore the influence of interatomic position fluctuation, we first assume a relative deviation ratio $\delta V/V$ with respect to the nonfluctuating interaction strength V by making the replacement

$$V \to V(1 + \delta V/V), \tag{12}$$

where $\delta V/V$ stands for the maximal deviation degree of the position fluctuation. For a determined $\delta V/V$ we extract a uniformly distributed random number generated from the range of $[-\delta V/V, +\delta V/V]$, which leads to a fluctuating interaction strength. Figures 3(a)–3(c) plot the average fidelity $\mathcal{F}$ versus the variation of $\delta V/V \in [0, 0.05]$. Such a deviation degree can also be changed in the view of two-atom distance fluctuation because $\sigma_r = (\delta V/V)r_0/6$ due to $V = C_6/r_0^6$ for a vdW interaction [72]. From Figs. 3(a)–3(c) it is apparent that, with an increasing deviation, the SWAP gate fidelity significantly decreases for the $q = 0$ case, e.g., when $\delta V/V = 0.05$ (equivalent to a position deviation of $\sigma_r \approx 40$ nm), $\mathcal{F}$ is decreased to approximately 0.87 with arbitrary pulse shapes. However, with the help of the modified antiblockade condition where q is optimized to minimize the time spent in $|rr\rangle$, the gate robustness against the deviation degree $\delta V/V$ can be greatly improved. The average gate fidelity $\mathcal{F}$ stays as high as approximately 0.97 for a large distance deviation.

Accounting for the fact that deviation in the Rydberg interaction between two atoms usually comes from the imperfections of atomic cooling and trapping, we consider the atoms with a finite temperature T and recalculate this position error. We assume that the relative position between two atoms satisfies a one-dimensional Gaussian distribution with its mean $r_0 = (C_6/V)^{1/6} \approx 4.8$ μm and standard deviation $\sigma_r = \sqrt{k_B T/m\omega^2}$ which varies with T. Here k_B, m, and ω mean the Boltzmann constant, the atomic mass, and the trapping frequency, respectively. By assuming $\omega/2\pi = 147$ kHz and $T = 20$ μK we can obtain $\sigma_r \approx 47.34$ nm and $\delta V/V \approx 5.92\%$. From the numerical results in Figs. 3(d)–3(f) it is clear that the gate infidelity $\mathcal{F}(T = 0) - \mathcal{F}(T)$ (excluding the decay error) for the modified antiblockade case is dramatically decreased. At the $T = 20$ μK accessible by a typical cold-atom experiment [73], we find that the gate infidelity due to the position error can sustain approximately 7.52×10^{-2}, which is almost a 50% reduction compared to that for the $q = 0$ case. A further expectation for decreasing the position error down to the level of approximately 10^{-3} may resort to lowering the temperature T or increasing the trapping frequency ω,

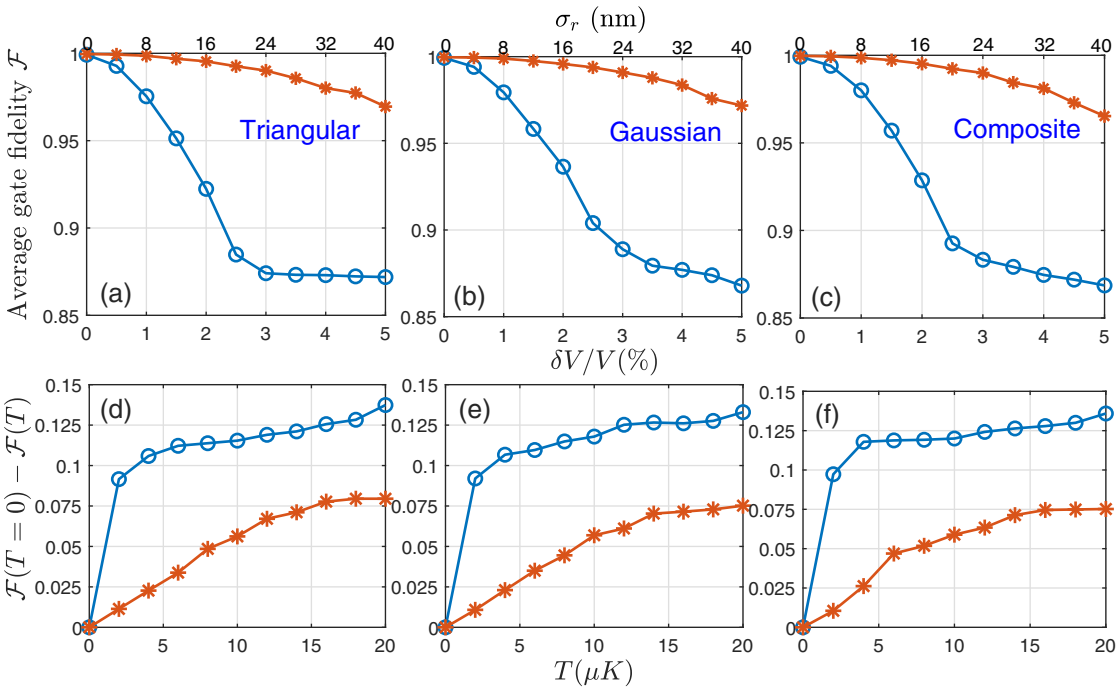

FIG. 3. (a)–(c) Average gate fidelity $\mathcal{F}$ as a function of the deviation degree of interaction strength $\delta V/V \in [0, 0.05]$ (equivalent to the position deviation $\sigma_r \in [0, 40]$ nm), where the decay from the Rydberg state is considered. (d)–(f) Gate infidelity $\mathcal{F}(T=0)-\mathcal{F}(T)$ for different atomic temperatures T, treated as one of the dominant error sources to produce an interaction deviation. Cases $q=0$ and $q\neq 0$ are presented by the blue line with circles and the red line with stars, respectively. Each point in (a)–(c) denotes an average of 300 uniformly distributed random samplings, while in (d)–(f) each point denotes an average of 300 Gaussian-distributed samplings for the atomic position. Pulse parameters used in the calculation are all obtained in the perfect case without any technical noise (case ii in Table I).

which allows for a smaller position deviation $\sigma_r < 14.7$ nm. Then the influence of position fluctuation on the infidelity can be suppressed to an experimentally accessible level approximately equal to 9.6×10^{-3}. Among the existing schemes of Rydberg antiblockade gates [74,75], our protocol reports the gate with the best position-error tolerance, thus moving one step closer to its experimental demonstration.

V. ROBUSTNESS AGAINST TECHNICAL IMPERFECTIONS

In this section we study the gate infidelity by taking into account other technical imperfections, as considered in a previous Rydberg experiment [76]. We restrict our analysis to the experimentally accessible Gaussian pulse (case ii), which possesses a smoother adjustment of the Rabi frequency as well as the best nonfluctuating (ideal) gate fidelity in the perfect case. Except for the position error explored in Sec. IV, other technical obstacles to a higher gate fidelity may involve the Doppler effect due to the atoms having a certain speed, the intensity and phase noises in excitation laser pulses, the relative position of atoms within a finite laser spatial width, etc. [77]. In the following we analyze in detail the influence of each contribution to the gate infidelity in order to give a conservative estimation for the gate performance.

A. Doppler dephasing

In a practical environment the qubit atoms would have a certain speed due to the residual thermal motion arising from the Doppler effect. The resulting laser frequency detuning experienced by the atoms will be slightly different from its desired value $\bar{\alpha}=0$, which gives rise to a modified one-atom Hamiltonian

$$\hat{\mathcal{H}}_j = \Omega_1 e^{-i(\Delta_1+\alpha_1)t}|0_j\rangle\langle r_j| + \Omega_2 e^{-i(\Delta_2+\alpha_2)t}|1_j\rangle\langle r_j| + \text{H.c.}, \tag{13}$$

where $\alpha_{1\,(2)} = \vec{k}_{1\,(2),\text{eff}}\cdot\vec{v}$ stands for an extra phase factor to the Rabi frequency and should fulfill a one-dimensional Gaussian distribution

$$f(\alpha_{1,2}) = \frac{1}{\sqrt{2\pi}\sigma_{\alpha_{1,2}}} e^{-(\alpha_{1,2}-\bar{\alpha})^2/2\sigma^2_{\alpha_{1,2}}} \tag{14}$$

with respect to the standard deviations $\sigma_{\alpha_1} = k_{1,\text{eff}}v_{\text{rms}}$ and $\sigma_{\alpha_2} = k_{2,\text{eff}}v_{\text{rms}}$. Here $T = 20$ μK corresponds to the one-dimensional rms velocity $v_{\text{rms}} = \sqrt{k_B T/m} \approx 44$ mm/s. In addition, we recall our setup shown in Fig. 1(insets) where both transitions $|0\rangle \to |r\rangle$ and $|1\rangle \to |r\rangle$ are mediated by two different low-lying p states. Therefore, the effective wave vectors are $k_{1,\text{eff}} = 8.76\times10^6$ m^{-1} and $k_{2,\text{eff}} = 5\times10^6$ m^{-1} when two excitation lasers have a counterpropagating configuration to minimize thermal Doppler shifts. That means for each measurement the extra frequency detuning $\alpha_{1,2}$ (except $\Delta_{1,2}$) of excitation lasers seen by the atoms is

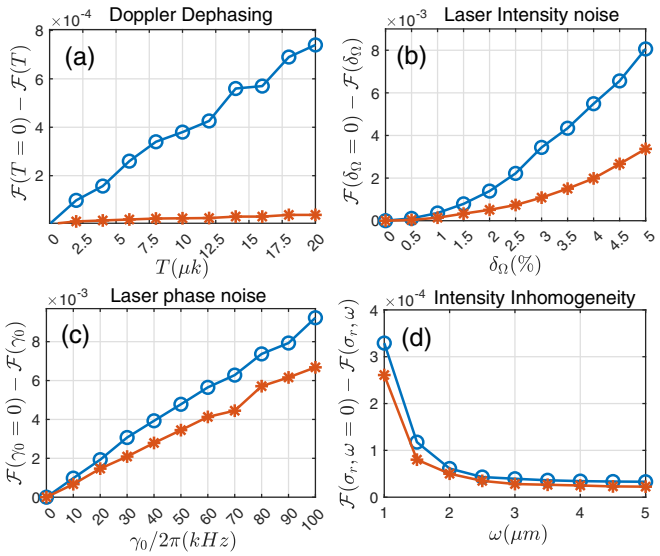

FIG. 4. Gate infidelity of the antiblockade SWAP gate with a pair of optimal Gaussian-shaped pulses (case ii), caused by (a) Doppler dephasing under different atomic temperatures $T \in [0, 20]$ μK, (b) laser intensity fluctuations $\delta_\Omega \in [0, 0.05]$, (c) laser phase fluctuations (characterized by a dephasing rate $\gamma_0/2\pi \in [0, 100]$ kHz for the ground-Rydberg transition), and (d) a laser beam waist $\omega \in [1, 5]$ μm where the standard deviation of the atomic position is fixed at $\sigma_r \approx 47.34$ nm at $T = 20$ μK. Similar to Fig. 3, numerical results based on the $q = 0$ case (blue line with circles) and the $q \neq 0$ case (red line with stars) are presented. Each point is obtained by an average of 300 samplings. Note that all simulation results depend on the choice of optimal pulse parameters in the perfect case (case ii in Table I).

a random value extracted from a centered Gaussian function $f(\alpha_{1,2})$ with maximal standard deviations $(\sigma_{\alpha_1}, \sigma_{\alpha_2}) = (0.383, 0.219)$ MHz. Numerical simulation allows for a new estimation of the gate infidelity $\mathcal{F}(T = 0) - \mathcal{F}(T)$, shown in Fig. 4(a) versus the atomic temperature T. By averaging over sufficient runs of measurement, the gate infidelity based on the modified antiblockade mechanism explicitly shows a dramatic reduction by one order of magnitude compared to that for the perfect antiblockade case. The reason is that $\alpha_{1\,(2)}$ serves as an extra and fluctuated detuning in addition to $\Delta_{1\,(2)}$, and the presence of an optimal q no doubt adds to the tolerance against the detuning deviation. We find that at $T = 20$ μK the infidelity caused by the Doppler dephasing has been suppressed to a negligible level approximately equal to 3.80×10^{-5} for the $q \neq 0$ case.

B. Laser intensity noise

In general, the laser intensity fluctuation coming from external technical weakness will lead to the deviation of desired excitation probability. In particular, a gate scheme that depends on pulse optimization requires an accurate knowledge of pulse parameters [78]. Here we introduce the same relative deviation $\delta_\Omega = \delta\Omega/\Omega_{1,2}^{\max}$ in the range of $\delta_\Omega \in [0, 0.05]$ with respect to the maximal Rabi frequency $\Omega_{1,2}^{\max}$. During each run of measurement the realistic laser Rabi frequency $\Omega_{1\,(2)}(t)$ should fluctuate by a uniform random number obtained from $[-\delta_\Omega, +\delta_\Omega]\Omega_{1\,(2)}^{\max}$ while the pulse shape is kept unchanged. Figure 4(b) shows the dependence of the gate infidelity on the laser intensity fluctuation. By increasing the relative deviation δ_Ω from 0% to 5.0%, the modified antiblockade case apparently has a better robustness to the laser intensity noise, although the gate infidelities remain at the level of approximately 10^{-3} in both cases.

C. Laser phase noise

The phases $\phi_{1,2}(t)$ of the laser Rabi frequency $\Omega_{1,2}(t)$ are random processes which should be characterized by a phase noise spectral density as a function of the Fourier frequency [79]. Since the laser phase noise caused by different frequencies involved in excitation lasers would lead to dephasing of Rabi oscillations [80–82], we describe the average result of the laser phase noise by introducing an extra Lindblad superoperator $\hat{\mathcal{L}}_d[\rho]$ in the master equation (9)

$$\hat{\mathcal{L}}_d[\rho] = \tfrac{1}{2}\sum_{j=1}^{4}[2\hat{\mathcal{L}}_{dj}\hat{\rho}\hat{\mathcal{L}}_{dj}^\dagger - (\hat{\mathcal{L}}_{dj}^\dagger\hat{\mathcal{L}}_{dj}\hat{\rho} + \hat{\rho}\hat{\mathcal{L}}_{dj}^\dagger\hat{\mathcal{L}}_{dj})], \quad (15)$$

with four dephasing channels expressed as

$$\hat{\mathcal{L}}_{d,1\,(2)} = \sqrt{\frac{\gamma_0}{2}}(|r\rangle_{1\,(2)}\langle r| - |0\rangle_{1\,(2)}\langle 0|),$$

$$\hat{\mathcal{L}}_{d,3\,(4)} = \sqrt{\frac{\gamma_0}{2}}(|r\rangle_{1\,(2)}\langle r| - |1\rangle_{1\,(2)}\langle 1|),$$

where γ_0 denotes a common dephasing rate. We have neglected the dephasing channel between $|r\rangle$ and $|\alpha\rangle$ since no laser pulse couples them. Figure 4(c) predicts the relationship between gate infidelity and different dephasing rates where $\gamma_0/2\pi \in [0, 0.1]$ MHz is considered. Here we set the maximal γ_0 to be $2\pi \times 0.1$ MHz at the same level as the experimental value [83]. For each γ_0 we adopt a uniform random value in the range of $[0, \gamma_0]$ and calculate the average infidelity $\mathcal{F}(\gamma_0 = 0) - \mathcal{F}(\gamma_0)$ after running 300 samplings. We observe that the effect of phase noise is more influential than that of the intensity noise, and the modified antiblockade condition can also slightly improve the gate tolerance. When $\gamma_0/2\pi = 0.1$ MHz the gate infidelity can achieve 6.68×10^{-3}, which also plays a non-negligible role compared to the dominant position error (approximately 10^{-2}).

D. Inhomogeneity in Rabi frequencies

In the above discussion we treat the thermal fluctuations of interatomic position in one dimension, which is also the propagation direction for two excitation lasers (see, e.g., Fig. 1 along $\hat{z}$). In fact, since lasers also have finite beam waists, such thermal fluctuations will simultaneously make the atoms deviate from the laser center in the $\hat{x}$-$\hat{y}$ plane. As a result, the actual laser intensity seen by the atoms would deviate from its ideal value, resulting in a position-dependent Rabi frequency only in the $\hat{x}$-$\hat{y}$ plane. As a consequence, the original time-dependent Rabi frequencies $\Omega_1(t)$ and $\Omega_2(t)$ should be modified by adding a space-dependent factor

$$\Omega_{1,2}(t, x, y) = \Omega_{1,2}(t, 0)e^{-x^2/w_x^2 - y^2/w_y^2}, \quad (16)$$

where $\Omega_{1,2}(t,0) = \Omega_{1,2}(t)$ is treated as the central Rabi frequency and $\omega_x = \omega_y = \omega$ is assumed to be a common beam waist. We have ignored the intensity inhomogeneity in the $\hat{z}$ direction because the position deviation σ_r of atoms is usually smaller than the Rayleigh length by orders of magnitude [77]. Furthermore, the position (x, y) of two atomic qubits in the $\hat{x}$-$\hat{y}$ plane is modeled by a two-dimensional Gaussian function with standard deviation $\sigma = \sigma_x = \sigma_y \approx 47.34$ nm at $T = 20$ μK. In Fig. 4(d) we tune the beam waist ω in the range of [1, 5] μm to see the effect of intensity inhomogeneity. Both cases clearly lead to similar gate infidelity values due to their comparable laser intensities. When $\omega > 2.0$ μm the influence can be lowered to less than 10^{-4}. However, if ω is narrowed to below 1.0 μm we find the infidelity has a dramatic increase because of the large intensity variations experienced by the atoms when the beam waist is too small. While accounting for the fact that the excitation laser can be focused typically to a wide waist of approximately 10 μm [84], this error can be totally negligible in the scheme.

VI. DISCUSSION

Ever since the pioneering works Refs. [85,86] proposed the idea of quantum computation with neutral atoms, many groups have focused on the experimental demonstration of various Rydberg quantum gates via the Rydberg blockade mechanism [87–89]. This method serves as the leading mainstream blueprint mainly because of its powerful insensitivity to the variation of interatomic interactions that fundamentally makes the position error negligible. In addition, another set of universal quantum gates based on the Rydberg antiblockade effect also emerges, since the first scheme by Carr and Saffman proposed a new method for preparing Rydberg entangled states via the combination of dissipative dynamics and antiblockade [7]. Nevertheless, such antiblockade gates require an exact knowledge of the interaction strength V and thus are very sensitive to the interaction deviation δV in practice. In this work we restricted our attention to the implementation of a two-qubit SWAP gate based on the antiblockade mechanism and showed that it is possible to improve the tolerance of gates to the position error caused by, e.g., residual thermal motion of atoms in the trapping region.

Table II summarizes the gate error budgeting of our protocol under different practical imperfections. Among them, although the dominant gate error remains the position fluctuation, e.g., it stays at the level of 10^{-2} for the $q \neq 0$ case, this value has been greatly decreased by at least one order of magnitude compared to that in the reported antiblockade-gate schemes [27,74,75,90]. In addition, our protocol suffers a higher sensitivity (approximately 10^{-3}) to the fluctuation of excitation lasers because of the pulse optimization. Other errors due to the finite radiative lifetime of Rydberg states, the Doppler dephasing, and the inhomogeneous Rabi frequency all make negligible contributions (10^{-5}–10^{-4}). After taking into into account all error sources, we can obtain a more conservative lower bound on the predicted gate fidelity $\mathcal{F} \geqslant 0.9143$. The potential for a higher-fidelity antiblockade gate can depend on a further improvement in the tolerance to the position fluctuation, especially by using the cooling method.

TABLE II. Error budget for case ii with optimal Gaussian pulses. As expected, among all obstacles (intrinsic and technical) the position error originating from fluctuations in the relative position between two atoms is the dominant error source. The Doppler dephasing and the inhomogeneity in laser Rabi frequencies are less important. Every error number is obtained via an average over 300 repeated measurements and the values in parentheses denote the maximal deviation. By considering all error sources simultaneously, we obtain very conservative estimates for the gate fidelity, which are $\mathcal{F} \geqslant 0.8482$ and $\mathcal{F} \geqslant 0.9143$, corresponding to the cases of $q = 0$ and $q \neq 0$, respectively.

Error sources	Error budget	
$q/2\pi$	0	5.037 MHz
Rydberg decay	7.31×10^{-4}	3.18×10^{-4}
Position fluctuation ($\sigma_r = 47.34$ nm)	1.33×10^{-1}	7.52×10^{-2}
Doppler dephasing ($T = 20$ μK)	7.39×10^{-4}	3.80×10^{-5}
Inhomogeneous Rabi frequency ($\omega = 2$ μm)	6.13×10^{-5}	5.02×10^{-5}
Laser intensity ($\delta_\Omega = 5.0\%$)	8.06×10^{-3}	3.37×10^{-3}
Laser phase ($\gamma_0/2\pi = 0.1$ MHz)	9.23×10^{-3}	6.68×10^{-3}

VII. CONCLUSION

We have shown that the modified antiblockade effect cooperating with pulse optimization can lead to Rydberg antiblockade SWAP gates with unprecedented tolerance, offering great promise for their experimental demonstration. Through optimization we found that the time spent in the double Rydberg state can be reduced by more than 70% compared to that in the perfect antiblockade case, which does not depend on the realistic shape of the laser pulses. For this reason the insensitivity of such gates to the position fluctuations can be improved by one order of magnitude, resulting in a quite competitive gate fidelity of $\mathcal{F} \geqslant 0.9143$ in the presence of significant position deviation for a practical temperature $T \sim 20$ μK. Larger gate tolerance may be achievable by using, e.g., a more adequate cooling technique [91], optimal three-dimensional geometric configuration [92], fault-tolerant nonadiabatic geometric quantum computation [93,94], and other advanced optimization algorithms [50]. The prospect for realizing fast and high-fidelity state swapping with gate-duration-optimized pulses is presented in Appendix B. We numerically confirm that an increase in the restriction of maximal Rabi frequency to be $2\pi \times 50$ MHz can increase the conservative gate fidelity to 0.9550 within an optimal gate time $T_g = 0.1177$ μs. Finally, the fast and high-fidelity SWAP gate can be used as a tool for other important applications in the frontier of quantum information science, for example, constructing scalable superconducting quantum processors [95].

ACKNOWLEDGMENTS

We acknowledge financial support from NSFC under Grants No. 12174106, No. 11474094, No. 11104076, No. 12274376, and No. 12304407; and from the Major science and technology projects of Henan Province under Grant No. 221100210400; and from Science and Technol-

ogy Commission of Shanghai Municipality under Grant No. 18ZR1412800.

APPENDIX A: DERIVATION OF THE EFFECTIVE HAMILTONIAN IN EQS. (4)–(6)

In this Appendix we illustrate the derivation of the effective Hamiltonians in Eqs. (4)–(6). We recall the total Hamiltonian of the system in (1), $\hat{\mathcal{H}} = \hat{\mathcal{H}}_1 \otimes \hat{\mathcal{I}}_2 + \hat{\mathcal{I}}_1 \otimes \hat{\mathcal{H}}_2 + \hat{V}_{rr}$, with $\hat{\mathcal{I}}_j$ a 3×3 identity matrix and $j = 1, 2$. Here the single-atom Hamiltonian in the Schrödinger picture reads

$$\hat{\mathcal{H}}_j = \sum_{i=0,1,r} \omega_i |i\rangle_j\langle i| + \Omega_1 |r\rangle_j\langle 0| e^{-i\omega_{l1}t} + \Omega_2 |r\rangle_j\langle 1| e^{-i\omega_{l2}t} + \text{H.c.}, \tag{A1}$$

where ω_i $(i = 0, 1, r)$ describes the frequency of the atomic level $|i\rangle$ and $\omega_{l1\,(l2)}$ represents the frequency of the optical driving fields. Turning to the interaction picture, with respect to a rotating frame we have

$$\hat{\mathcal{H}}_j = \Omega_1 e^{-i\Delta_1 t} |r\rangle_j\langle 0| + \Omega_2 e^{-i\Delta_2 t} |r\rangle_j\langle 1| + \text{H.c.}, \tag{A2}$$

where we introduce the detuning parameters $\Delta_1 = \omega_{l1} - (\omega_r - \omega_0)$ and $\Delta_2 = \omega_{l2} - (\omega_r - \omega_1)$ for simplicity. In addition, the third term in (1),

$$\hat{V}_{rr} = V |rr\rangle\langle rr|, \tag{A3}$$

is the Rydberg-mediated interaction as two atoms simultaneously occupy the Rydberg state, with $V = C_6/r_0^6$ the vdW interaction strength.

To simplify the calculation, we first turn to the frame of two-atom basis states in which the above single-atom Hamiltonian $\hat{\mathcal{H}}_j$ could be reexpressed as

$$\hat{\mathcal{H}}_1 = \Omega_1 e^{-i\Delta_1 t}(|r1\rangle\langle 01| + |r0\rangle\langle 00| + |rr\rangle\langle 0r|) + \Omega_2 e^{-i\Delta_2 t}(|r1\rangle\langle 11| + |r0\rangle\langle 10| + |rr\rangle\langle 1r|) + \text{H.c.}, \tag{A4}$$

$$\hat{\mathcal{H}}_2 = \Omega_1 e^{-i\Delta_1 t}(|1r\rangle\langle 10| + |0r\rangle\langle 00| + |rr\rangle\langle r0|) + \Omega_2 e^{-i\Delta_2 t}(|1r\rangle\langle 11| + |0r\rangle\langle 01| + |rr\rangle\langle r1|) + \text{H.c.}, \tag{A5}$$

with which the total Hamiltonian (1) of the system reduces to

$$\hat{\mathcal{H}} = \hat{\mathcal{H}}_1 + \hat{\mathcal{H}}_2 + \hat{V}_{rr}. \tag{A6}$$

To demonstrate the role of the Rydberg-mediated interaction, we rotate $\hat{\mathcal{H}}$ in (A6) with respect to a unitary operator $\hat{U} = \exp[-i(\Delta_1 + \Delta_2)t|rr\rangle\langle rr|]$, which leads to

$$\hat{\mathcal{H}}' = \hat{U}^\dagger \hat{\mathcal{H}} \hat{U} + i\hbar \frac{\partial \hat{U}^\dagger}{\partial t} \hat{U} = \hat{\mathcal{H}}_0 + \hat{\mathcal{H}}_I, \tag{A7}$$

where the products are given by

$$\begin{aligned}
\hat{\mathcal{H}}_0 = {} & \Omega_1 e^{-i\Delta_1 t}(|r1\rangle\langle 01| + |r0\rangle\langle 00|) + \Omega_1 e^{i\Delta_2 t}|rr\rangle\langle 0r| \\
& + \Omega_2 e^{-i\Delta_2 t}(|r1\rangle\langle 11| + |r0\rangle\langle 10|) + \Omega_2 e^{i\Delta_1 t}|rr\rangle\langle 1r| \\
& + \Omega_2 e^{-i\Delta_2 t}(|0r\rangle\langle 01| + |1r\rangle\langle 11|) + \Omega_2 e^{i\Delta_1 t}|rr\rangle\langle r1| \\
& + \Omega_1 e^{-i\Delta_1 t}(|0r\rangle\langle 00| + |1r\rangle\langle 10|) + \Omega_1 e^{i\Delta_2 t}|rr\rangle\langle r0|) \\
& + \text{H.c.}, \\
\hat{\mathcal{H}}_I = {} & (V - \Delta_1 - \Delta_2)|rr\rangle\langle rr|.
\end{aligned}$$

We aim at using the laser detuning to compensate for the energy shift induced by the Rydberg-mediated interaction so that it satisfies $V = \Delta_1 + \Delta_2 + q$, yielding $\hat{\mathcal{H}}_I = q|rr\rangle\langle rr|$, which ensures a nearly resonant two-photon transition with respect to $|rr\rangle$. Clearly, when $q = 0$ it means the perfect antiblockade condition in which we can arrange both atoms to be excited to the Rydberg state. If q is a nonzero value it represents the modified antiblockade which can modify the performance of some unwanted ac Stark shift and be effectively used for a SWAP gate task.

Next we rewrite the Hamiltonian $\hat{\mathcal{H}}_0$ in a more universal form

$$\hat{\mathcal{H}}_0 = \sum_{n=1,2} \hat{h}_n^\dagger e^{i\Delta_n t} + \hat{h}_n e^{-i\Delta_n t} \tag{A8}$$

in which $\hat{h}_1$ and $\hat{h}_2$ take exact forms

$$\begin{aligned}
\hat{h}_1 = {} & \Omega_1(|r1\rangle\langle 01| + |r0\rangle\langle 00| + |0r\rangle\langle 00| + |1r\rangle\langle 10|) \\
& + \Omega_2(|1r\rangle\langle rr| + |r1\rangle\langle rr|), \\
\hat{h}_2 = {} & \Omega_2(|0r\rangle\langle 01| + |1r\rangle\langle 11| + |r1\rangle\langle 11| + |r0\rangle\langle 10|) \\
& + \Omega_1(|0r\rangle\langle rr| + |r0\rangle\langle rr|).
\end{aligned} \tag{A9}$$

Furthermore, if the parameters satisfy $|\Delta_1| \gg \Omega_1^{\max}$ and $|\Delta_2| \gg \Omega_2^{\max}$ (large-detuning assumption), it is convenient to get a direct two-photon transition between $|rr\rangle$ and $|01\rangle$ $(|10\rangle)$ with other singly-excited Rydberg states strongly suppressed for large detunings. Here we confine our interest to the dynamics which are time averaged over a longer period than any oscillation periods [96]. So after neglecting all oscillation terms proportional to $e^{i(\Delta_n \pm \Delta_m)t}$ $(n \neq m)$, we finally arrive at a simple effective form for $\hat{\mathcal{H}}_0$ [97],

$$\hat{\mathcal{H}}_{0,\text{eff}} = \frac{1}{\Delta_1}[\hat{h}_1^\dagger, \hat{h}_1] + \frac{1}{\Delta_2}[\hat{h}_2^\dagger, \hat{h}_2]. \tag{A10}$$

By inserting Eq. (A9) into (A10) the effective Hamiltonian can be changed to

$$\begin{aligned}
\hat{\mathcal{H}}_{0,\text{eff}} = {} & -\left(\frac{\Omega_1^2}{\Delta_1} + \frac{\Omega_1^2}{\Delta_2}\right)|r0\rangle\langle 0r| - \left(\frac{\Omega_1^2}{\Delta_1} + \frac{\Omega_1^2 + \Omega_2^2}{\Delta_2}\right)(|r0\rangle\langle r0| + |0r\rangle\langle 0r|) - \left(\frac{\Omega_2^2}{\Delta_1} + \frac{\Omega_2^2}{\Delta_2}\right)|r1\rangle\langle 1r| \\
& - \left(\frac{\Omega_2^2}{\Delta_2} + \frac{\Omega_1^2 + \Omega_2^2}{\Delta_1}\right)(|r1\rangle\langle r1| + |1r\rangle\langle 1r|) + \left(\frac{\Omega_1\Omega_2}{\Delta_1} + \frac{\Omega_1\Omega_2}{\Delta_2}\right)(|rr\rangle\langle 01| + |rr\rangle\langle 10|) \\
& + \left(\frac{\Omega_1^2}{\Delta_1} + \frac{\Omega_2^2}{\Delta_2}\right)(|01\rangle\langle 01| + |10\rangle\langle 10|) + \frac{2\Omega_1^2}{\Delta_1}|00\rangle\langle 00| + \frac{2\Omega_2^2}{\Delta_2}|11\rangle\langle 11| + \left(\frac{2\Omega_2^2}{\Delta_1} + \frac{2\Omega_1^2}{\Delta_2}\right)|rr\rangle\langle rr| + \text{H.c.}
\end{aligned} \tag{A11}$$

Via following Eq. (A11), we observe that the singly-excited states such as $\{|0r\rangle, |r0\rangle, |1r\rangle, |r1\rangle\}$ are now in a closed subspace and decoupled to the initial states $\{|00\rangle, |01\rangle, |10\rangle, |11\rangle\}$ due to the assumption of large laser detunings. So it is safe to drop these trivial terms and the total Hamiltonian $\hat{\mathcal{H}}'$ can be effectively described by

$$\begin{aligned}\hat{\mathcal{H}}'_{\rm eff} &= \hat{\mathcal{H}}'_{0,\rm eff} + \hat{\mathcal{H}}_I \\ &= \left(\frac{\Omega_1\Omega_2}{\Delta_1} + \frac{\Omega_1\Omega_2}{\Delta_2}\right)(|rr\rangle\langle 01| + |rr\rangle\langle 10|) + \text{H.c.} \\ &\quad + \left(\frac{\Omega_1^2}{\Delta_1} + \frac{\Omega_2^2}{\Delta_2}\right)(|01\rangle\langle 01| + |10\rangle\langle 10|) + \frac{2\Omega_1^2}{\Delta_1}|00\rangle\langle 00| \\ &\quad + \frac{2\Omega_2^2}{\Delta_2}|11\rangle\langle 11| + \left(\frac{2\Omega_2^2}{\Delta_1} + \frac{2\Omega_1^2}{\Delta_2} + q\right)|rr\rangle\langle rr|.\end{aligned} \tag{A12}$$

Based on Eq. (A12), one can see that the collective ground state $|00\rangle$ or $|11\rangle$ stays decoupled, resulting in

$$\hat{\mathcal{H}}_{00,\rm eff} = \frac{2\Omega_1^2}{\Delta_1}|00\rangle\langle 00| \text{ or } \hat{\mathcal{H}}_{11,\rm eff} = \frac{2\Omega_2^2}{\Delta_2}|11\rangle\langle 11| \tag{A13}$$

for the initialization of states $|00\rangle$ and $|11\rangle$. However, when the initial state is $|01\rangle$ (equivalent to $|10\rangle$) one has

$$\begin{aligned}\hat{\mathcal{H}}_{01,\rm eff} &= \left(\frac{\Omega_1\Omega_2}{\Delta_1} + \frac{\Omega_1\Omega_2}{\Delta_2}\right)(|rr\rangle\langle 01| + |01\rangle\langle rr|) + \text{H.c.} \\ &\quad + \left(\frac{2\Omega_2^2}{\Delta_1} + \frac{2\Omega_1^2}{\Delta_2} + q\right)|rr\rangle\langle rr| \\ &\quad + \left(\frac{\Omega_1^2}{\Delta_1} + \frac{\Omega_2^2}{\Delta_2}\right)(|01\rangle\langle 01| + |10\rangle\langle 10|).\end{aligned} \tag{A14}$$

It is worthwhile to stress that although the $\hat{\mathcal{H}}_{01,\rm eff}$ involves the required swapping dynamics between two target states $|01\rangle$ and $|10\rangle$, it is clearly mediated by the double Rydberg state $|rr\rangle$ because of the antiblockade facilitation, increasing its sensitivity to the position error. Luckily, the presence of the factor q ($\neq 0$) can modify the Stark shift with respect to $|rr\rangle$, suppressing the population on it by using an off-resonance detuning. This makes the resulting gate insusceptible to the interaction fluctuation. In addition, the ac Stark shift to the ground states $|01\rangle$ and $|10\rangle$ [the last term in Eq. (A14)] would no doubt influence the swapping dynamics. Applying auxiliary atom-field couplings to overcome it, as done in [44], may increase the experimental complexity. We identify that the type of pulse optimization in our protocol can minimize this influence without auxiliary fields, promising for a high-fidelity SWAP gate with improved robustness. Finally, note that our protocol, which benefits from the combination of the modified antiblockade effect and the pulse optimization, is promising for other two-qubit quantum gates with a different pulse design. For example, a controlled-NOT (CNOT) gate requires an asymmetric pulse driving in which atom 1 is only driven by $\Omega_2(t)$ for the $|1\rangle \to |r\rangle$ transition, leaving $|0\rangle$ idle. In this case the antiblockade facilitation could allow for an effective coupling between $|10\rangle$ and $|11\rangle$, achieving a robust two-qubit CNOT gate.

APPENDIX B: ACHIEVING FAST STATE SWAPPING WITH PULSE OPTIMIZATION

In this Appendix we provide extended calculations for a fast swapping operation in practice. Inspired by the methods used in [98], we find that when the gate duration T_g is also varied, serving as another ancillary optimal parameter, the SWAP gate performance can be further improved with a higher tolerance. To show the role of T_g optimization we focus on two cases: one with a restriction of $(\Omega_1^{\max}, \Omega_2^{\max})/2\pi \leqslant 10$ MHz and a second with $(\Omega_1^{\max}, \Omega_2^{\max})/2\pi \leqslant 50$ MHz. Such choices will lead to approximate timescale levels for the gate duration, which are 1.0 and 0.1 μs for maintaining complete circles of rotation. Note that when we vary the pulse parameters, a simultaneous optimization for the gate duration can also minimize the time spent in the Rydberg state.

In this extended calculation all parameters including T_g are tunable so as to maximize the perfect gate fidelity in the absence of any technical noise. To be specific, we also extend the simplified model in Fig. 1 by using different branching ratios with the leakage state $|\alpha\rangle$, which are $\eta_{r\to 1} = \frac{1}{8}$, $\eta_{r\to 2} = \frac{1}{8}$, and $\eta_{r\to\alpha} = \frac{3}{4}$. State $|\alpha\rangle$ represents all ground magnetic sublevels $|5S_{1/2}, F = 1, m_F = \pm 1\rangle$ and $|5S_{1/2}, F = 2, m_F = \pm 1, \pm 2\rangle$ except $|0\rangle$ and $|1\rangle$. In this practical situation we find that the success of the optimization is not affected by the increase of parameters to be optimized. Finally, we obtain two sets of new parameters for the gate,

$$\begin{aligned}(q, \Delta_1, \Delta_2)/2\pi &= (6.051, 22.951, 41.488)\ \text{MHz}, \\ \left(\Omega_1^{\max}, \Omega_2^{\max}\right)/2\pi &= (4.969, 9.728)\ \text{MHz}, \\ (\omega_1, \omega_2) &= (0.4948, 0.5318)\ \mu\text{s}, \\ T_g &= 0.8894\ \mu s;\end{aligned} \tag{B1}$$

$$\begin{aligned}(q, \Delta_1, \Delta_2)/2\pi &= (33.429, -94.133, 131.194)\ \text{MHz}, \\ \left(\Omega_1^{\max}, \Omega_2^{\max}\right)/2\pi &= (37.413, 48.404)\ \text{MHz}, \\ (\omega_1, \omega_2) &= (0.0586, 1.6082)\ \mu\text{s}, \\ T_g &= 0.1177\ \mu s,\end{aligned} \tag{B2}$$

corresponding to the restrictions $\Omega_{1\,(2)}^{\max}/2\pi \leqslant 10$ and 50 MHz, respectively, set for the numerical optimization.

In Figs. 5(a) and 5(b) we show the optimal pulse shapes $\Omega_1(t)$ and $\Omega_2(t)$ as well as the corresponding population dynamics. As compared to the case in Figs. 2(a 5)–2(e 5), we find that, together with the optimization for T_g, the time spent on $|rr\rangle$ could be slightly shortened to $T_{rr} \approx 0.0216$ μs owing to the use of a small and optimal $T_g = 0.8894$ μs (less than 1.0 μs). The perfect gate fidelity stays at a high level of $\mathcal{F} \approx 0.999\,484$, although this value is slightly smaller than the observed one $\mathcal{F} \approx 0.999\,682$ in case ii ($q \neq 0$, Table I) because the population loss caused by the leakage state $|\alpha\rangle$ is irreversible. In addition, note that if the restriction for $\Omega_{1\,(2)}^{\max}$ is increased to $2\pi \times 50$ MHz, the T_g required can be lowered to 0.1177 μs, in excellent agreement with the relationship between $\Omega_{1\,(2)}^{\max}$ and T_g. From the error budget in Table III, it is apparent that the Rydberg decay representing the dominant source of error for the perfect gate fidelity cannot be easily affected by shortening the gate duration. Therefore, the state swapping fidelity in the perfect case is almost the same. How-

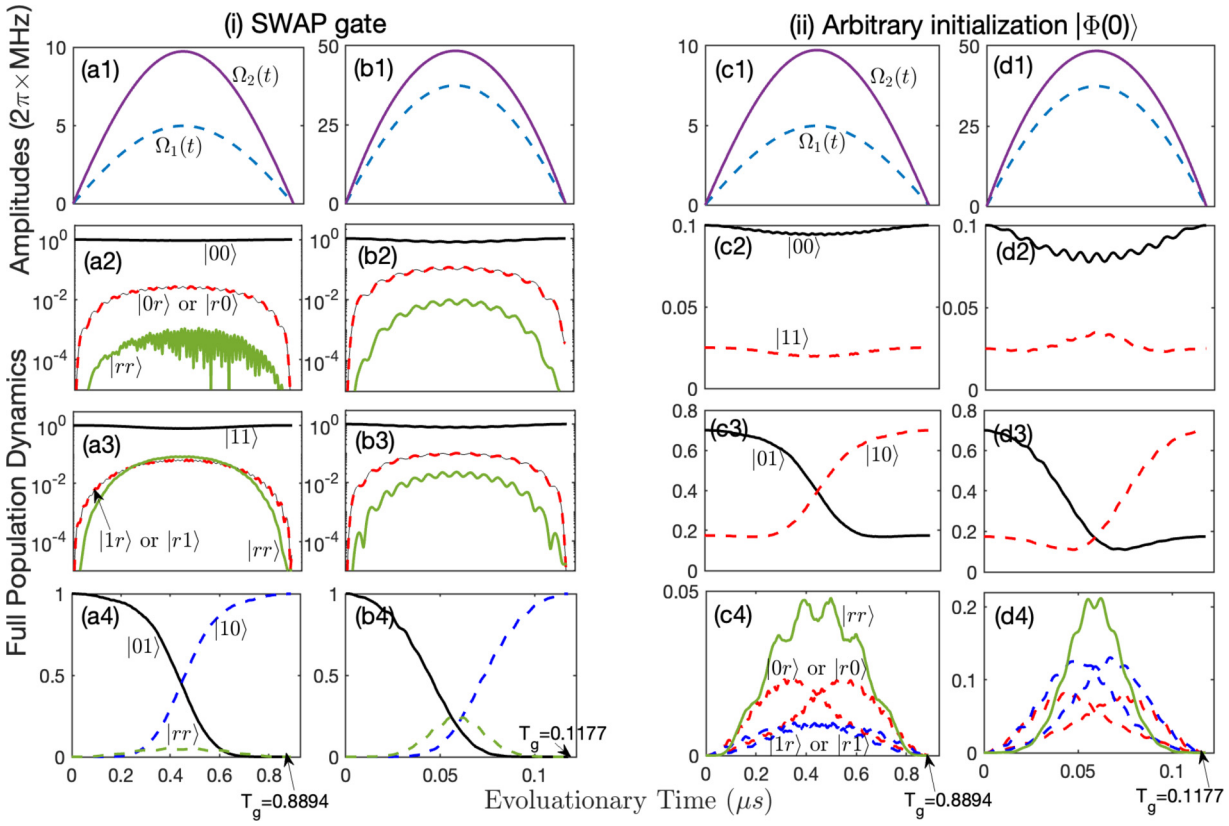

FIG. 5. Optimal Gaussian pulse shapes and the full population dynamics based on (a) and (b) the SWAP gate protocol and (c) and (d) an arbitrary initialization $|\Phi(0)\rangle = \frac{1}{\sqrt{10}}|00\rangle + \sqrt{\frac{7}{10}}|01\rangle + \sqrt{\frac{7}{40}}|10\rangle + \frac{1}{\sqrt{40}}|11\rangle$. By constraining the maximal Rabi frequencies $(\Omega_1^{\max}, \Omega_2^{\max})$ to be (a) and (c) $2\pi \times 10$ MHz and (b) and (d) $2\pi \times 50$ MHz, the optimal gate durations are $T_g = 0.8894$ μs and 0.1177 μs, correspondingly. All line types are labeled in (a) and (c).

ever, for a shorten gate duration at the expense of higher Rabi frequency, the time T_{rr} is able to decrease by one order of magnitude ($T_{rr} \approx 0.0085$ μs), which can no doubt make the gate more susceptible to other technical imperfections. As shown in Table III, the gate tolerance to the position fluctuation is explicitly improved ($6.98 \times 10^{-2} \rightarrow 1.15 \times 10^{-2}$) owing to the suppression of the Rydberg-state duration. The only worse effect comes from the laser intensity fluctuation because it increases with the values of $\Omega_1^{\max}$ and $\Omega_2^{\max}$. For a fast state swapping operation the laser intensity noise will play an equivalently important role as the position fluctuation. By taking into account different technical imperfections limiting the gate fidelity, we finally demonstrate that a conservative fidelity for the fast SWAP protocol above 0.9550 is achievable.

In order to show the SWAP gate that can be used for an arbitrary state swapping we introduce a normalized two-qubit

TABLE III. Error budget for the two-qubit SWAP gate and for an arbitrary initialization $|\Phi(0)\rangle$. From left to right the numerical simulations are performed at different branching ratios or different T_g values, corresponding to the cases graphically plotted in Figs. 2(a 5)–2(e 5), 5(a), 5(b), 5(c), and 5(d), respectively. The perfect fidelity is only contributed by the Rydberg decay error. A more conservative estimation for the state swapping fidelity is given, accounting for the sum of all intrinsic and technical error sources.

Error sources	Error budget (SWAP)			Error budget $\|\Phi(0)\rangle$	
Branching ratios $(\eta_{r\to1}, \eta_{r\to2}, \eta_{r\to\alpha})$	$(\frac{1}{2}, \frac{1}{2}, 0)$	$(\frac{1}{8}, \frac{1}{8}, \frac{3}{4})$	$(\frac{1}{8}, \frac{1}{8}, \frac{3}{4})$	$(\frac{1}{8}, \frac{1}{8}, \frac{3}{4})$	$(\frac{1}{8}, \frac{1}{8}, \frac{3}{4})$
$q/2\pi$ (MHz)	5.037	6.051	33.429	6.051	33.429
T_g (μs)	1.0	0.8894	0.1177	0.8894	0.1177
Rydberg decay	3.18×10^{-4}	5.16×10^{-4}	4.58×10^{-4}	4.97×10^{-4}	5.83×10^{-4}
Position fluctuation ($\sigma_r = 47.34$ nm)	7.52×10^{-2}	6.98×10^{-2}	1.15×10^{-2}	2.78×10^{-2}	1.01×10^{-3}
Doppler dephasing ($T = 20$ μK)	3.80×10^{-5}	1.58×10^{-5}	1.22×10^{-5}	8.00×10^{-6}	2.76×10^{-5}
Inhomogeneous Rabi frequency ($\omega = 2$ μm)	5.02×10^{-5}	1.24×10^{-5}	2.76×10^{-5}	3.00×10^{-6}	2.74×10^{-6}
Laser intensity ($\delta_\Omega = 5.0\%$)	3.37×10^{-3}	3.11×10^{-3}	3.11×10^{-2}	2.47×10^{-4}	1.73×10^{-2}
Laser phase ($\gamma_0/2\pi = 100$ kHz)	6.68×10^{-3}	6.82×10^{-3}	1.94×10^{-3}	5.23×10^{-3}	2.07×10^{-3}
State swapping fidelity (perfect)	0.9997	0.9995	0.9995	0.9995	0.9994
State swapping fidelity (conservative)	0.9140	0.9200	0.9550	0.9662	0.9790

state serving as the initial state

$$|\Psi(0)\rangle = A_{00}|00\rangle + A_{01}|01\rangle + A_{10}|10\rangle + A_{11}|11\rangle, \quad \text{(B3)}$$

with $\sum_{i,j} |A_{i,j}|^2 = 1$ and $i, j \in \{0, 1\}$. Such arbitrariness of the initialization can be used to study the fast state swapping of the scheme. Ideally, for an arbitrary initialization $|\Phi(0)\rangle$ the output state should be $|\Psi(T_g)\rangle = A_{00}|00\rangle + A_{10}|01\rangle + A_{01}|10\rangle + A_{11}|11\rangle$. Here we modify the definition of average fidelity in Eq. (11) as

$$\mathcal{F} = \mathrm{Tr}\sqrt{\sqrt{U}\rho(t = T_g)\sqrt{U}} \quad \text{(B4)}$$

because the initial state $|\Phi(0)\rangle$ is individually normalized. Here ρ is the practical density matrix at measured time $t = T_g$ and $U = |\Phi(0)\rangle\langle\Phi(0)|$ is the ideal swapping matrix. In Figs. 5(c) and 5(d) we comparable the time-dependent evolution of different populations $|A_{i,j}(t)|^2$ for state $|ij\rangle$ by adopting the optimization parameters in (B1) and (B2). A complete error budget is presented in the last two columns of Table III. In general, a fast and high-fidelity state swapping is achievable for an arbitrary initialization. The swapping fidelity considered for a nonfluctuating environment (perfect case) can remain at a high value 0.9995(4) owing to the success of pulse optimization. In contrast, taking into account various technical limitations from a typical Rydberg experimental setup, we find that the position fluctuation and the laser intensity noise are still two dominant contributions, the same as in the SWAP gate protocol. However, the greatest influence from a fluctuating position has been lowered to 1.01×10^{-3} because of the relatively small population in two swapping states $|01\rangle$ and $|10\rangle$. Nevertheless, the laser intensity noise plays the most important role because the maximal Rabi frequency to be optimized has reached $2\pi \times 48.404$ MHz for $\Omega_2^{\max}$. After considering the technical noises, a conservative estimation for the predicted fidelity of state swapping can achieve 0.9662 and 0.9790. It is worthwhile to note that achieving fast quantum state operations within a submicrosecond duration has promising advantages deserving more theoretical and experimental efforts in the future.

[1] M. Saffman, Quantum computing with atomic qubits and Rydberg interactions: Progress and challenges, J. Phys. B **49**, 202001 (2016).

[2] L. Henriet, L. Beguin, A. Signoles, T. Lahaye, A. Browaeys, G. Reymond, and C. Jurczak, Quantum computing with neutral atoms, Quantum **4**, 327 (2020).

[3] M. Morgado and S. Whitlock, Quantum simulation and computing with Rydberg-interacting qubits, AVS Quantum Science **3**, 023501 (2021).

[4] I. Cong, H. Levine, A. Keesling, D. Bluvstein, S. Wang, and M. Lukin, Hardware-efficient, fault-tolerant quantum computation with Rydberg atoms, Phys. Rev. X **12**, 021049 (2022).

[5] X. Shi, Quantum logic and entanglement by neutral Rydberg atoms: Methods and fidelity, Quantum Sci. Technol. **7**, 023002 (2022).

[6] T. Graham, Y. Song, J. Scott, C. Poole, L. Phuttitarn, K. Jooya, P. Eichler, X. Jiang, A. Marra, B. Grinkemeyer *et al.*, Multi-qubit entanglement and algorithms on a neutral-atom quantum computer, Nature (London) **604**, 457 (2022).

[7] A. Carr and M. Saffman, Preparation of entangled and antiferromagnetic states by dissipative Rydberg pumping, Phys. Rev. Lett. **111**, 033607 (2013).

[8] X. Shao, J. You, T. Zheng, C. Oh, and S. Zhang, Stationary three-dimensional entanglement via dissipative Rydberg pumping, Phys. Rev. A **89**, 052313 (2014).

[9] S. Su, Q. Guo, H. Wang, and S. Zhang, Simplified scheme for entanglement preparation with Rydberg pumping via dissipation, Phys. Rev. A **92**, 022328 (2015).

[10] G. Barontini, L. Hohmann, F. Haas, J. Estève, and J. Reichel, Deterministic generation of multiparticle entanglement by quantum Zeno dynamics, Science **349**, 1317 (2015).

[11] X. Chen, H. Xie, G. Lin, X. Shang, M. Ye, and X. Lin, Dissipative generation of a steady three-atom singlet state based on Rydberg pumping, Phys. Rev. A **96**, 042308 (2017).

[12] Y. Zhao, B. Liu, Y. Ji, S. Tang, and X. Shao, Robust generation of entangled state via ground-state antiblockade of Rydberg atoms, Sci. Rep. **7**, 16489 (2017).

[13] Y. Chen, Z. Shi, J. Song, Y. Xia, and S. Zheng, Accelerated and noise-resistant generation of high-fidelity steady-state entanglement with Rydberg atoms, Phys. Rev. A **97**, 032328 (2018).

[14] T. Wintermantel, Y. Wang, G. Lochead, S. Shevate, G. Brennen, and S. Whitlock, Unitary and nonunitary quantum cellular automata with Rydberg arrays, Phys. Rev. Lett. **124**, 070503 (2020).

[15] F. Gambetta, C. Zhang, M. Hennrich, I. Lesanovsky, and W. Li, Long-range multibody interactions and three-body antiblockade in a trapped Rydberg ion chain, Phys. Rev. Lett. **125**, 133602 (2020).

[16] S. Mallavarapu, A. Niranjan, W. Li, S. Wüster, and R. Nath, Population trapping in a pair of periodically driven Rydberg atoms, Phys. Rev. A **103**, 023335 (2021).

[17] M. Malinowski, C. Zhang, V. Negnevitsky, I. Rojkov, F. Reiter, T. Nguyen, M. Stadler, D. Kienzler, K. Mehta, and J. Home, Generation of a maximally entangled state using collective optical pumping, Phys. Rev. Lett. **128**, 080503 (2022).

[18] T. Ates, T. Pohl and J. Rost, Antiblockade in Rydberg excitation of an ultracold lattice gas, Phys. Rev. Lett. **98**, 023002 (2007).

[19] T. Amthor, C. Giese, C. Hofmann, and M. Weidemüller, Evidence of antiblockade in an ultracold Rydberg gas, Phys. Rev. Lett. **104**, 013001 (2010).

[20] S. Bai, X. Tian, X. Han, Y. Jiao, J. Wu, J. Zhao, and S. Jia, Distinct antiblockade features of strongly interacting Rydberg atoms under a two-color weak excitation scheme, New J. Phys. **22**, 013004 (2020).

[21] M. Saffman and T. Walker, Analysis of a quantum logic device based on dipole-dipole interactions of optically trapped Rydberg atoms, Phys. Rev. A **72**, 022347 (2005).

[22] W. Li, C. Ates, and I. Lesanovsky, Nonadiabatic motional effects and dissipative blockade for Rydberg atoms excited from optical lattices or microtraps, Phys. Rev. Lett. **110**, 213005 (2013).

[23] X. Shi and T. Kennedy, Annulled van der Waals interaction and fast Rydberg quantum gates, Phys. Rev. A **95**, 043429 (2017).

[24] F. Robicheaux, T. Graham, and M. Saffman, Photon-recoil and laser-focusing limits to Rydberg gate fidelity, Phys. Rev. A **103**, 022424 (2021).

[25] S. de Léséleuc, D. Barredo, V. Lienhard, A. Browaeys, and T. Lahaye, Analysis of imperfections in the coherent optical excitation of single atoms to Rydberg states, Phys. Rev. A **97**, 053803 (2018).

[26] S. Su, Y. Tian, H. Shen, H. Zang, E. Liang, and S. Zhang, Applications of the modified Rydberg antiblockade regime with simultaneous driving, Phys. Rev. A **96**, 042335 (2017).

[27] J. Wu, Y. Wang, J. Han, Y. Feng, S. Su, Y. Xia, Y. Jiang, and J. Song, One-step implementation of Rydberg-antiblockade swap and controlled-swap gates with modified robustness, Photon. Res. **9**, 814 (2021).

[28] A. Kaufman, B. Lester, and C. Regal, Cooling a single atom in an optical tweezer to its quantum ground state, Phys. Rev. X **2**, 041014 (2012).

[29] J. Hu, A. Urvoy, Z. Vendeiro, V. Crépel, W. Chen, and V. Vuletić, Creation of a Bose-condensed gas of ^{87}Rb by laser cooling, Science **358**, 1078 (2017).

[30] C. Hölzl, A. Götzelmann, M. Wirth, M. Safronova, S. Weber, and F. Meinert, Motional ground-state cooling of single atoms in state-dependent optical tweezers, Phys. Rev. Res. **5**, 033093 (2023).

[31] J. Yang, X. He, R. Guo, P. Xu, K. Wang, C. Sheng, M. Liu, J. Wang, A. Derevianko, and M. Zhan, Coherence preservation of a single neutral atom qubit transferred between magic-intensity optical traps, Phys. Rev. Lett. **117**, 123201 (2016).

[32] A. Pagano, S. Weber, D. Jaschke, T. Pfau, F. Meinert, S. Montangero, and H. P. Büchler, Error budgeting for a controlled-phase gate with strontium-88 Rydberg atoms, Phys. Rev. Res. **4**, 033019 (2022).

[33] W. Feng and D. Wang, Quantum Fredkin gate based on synthetic three-body interactions in superconducting circuits, Phys. Rev. A **101**, 062312 (2020).

[34] M. Riebe, T. Monz, K. Kim, A. Villar, P. Schindler, M. Chwalla, M. Hennrich, and R. Blatt, Deterministic entanglement swapping with an ion-trap quantum computer, Nat. Phys. **4**, 839 (2008).

[35] X. Ma, S. Zotter, J. Kofler, R. Ursin, T. Jennewein, Č. Brukner, and A. Zeilinger, Experimental delayed-choice entanglement swapping, Nat. Phys. **8**, 479 (2012).

[36] W. Ning, X.-J. Huang, P.-R. Han, H. Li, H. Deng, Z.-B. Yang, Z.-R. Zhong, Y. Xia, K. Xu, D. Zheng, and S.-B. Zheng, Deterministic entanglement swapping in a superconducting circuit, Phys. Rev. Lett. **123**, 060502 (2019).

[37] N. Sangouard, C. Simon, H. Riedmatten, and N. Gisin, Quantum repeaters based on atomic ensembles and linear optics, Rev. Mod. Phys. **83**, 33 (2011).

[38] I. Tillman, A. Rubenok, S. Guha, and K. Seshadreesan, Supporting multiple entanglement flows through a continuous-variable quantum repeater, Phys. Rev. A **106**, 062611 (2022).

[39] Y. Chahine, I. Nemitz, and J. Lekki, Protocol for suppression of noise from stimulated multiphoton emissions in concatenated entanglement swapping links and quantum repeaters, Phys. Rev. A **108**, 022609 (2023).

[40] H. Levine, A. Keesling, G. Semeghini, A. Omran, T. Wang, S. Ebadi, H. Bernien, M. Greiner, V. Vuletić, H. Pichler, and M. Lukin, Parallel implementation of high-fidelity multiqubit gates with neutral atoms, Phys. Rev. Lett. **123**, 170503 (2019).

[41] N. Šibalić, J. Pritchard, C. Adams, and K. Weatherill, ARC: An open-source library for calculating properties of alkali Rydberg atoms, Comput. Phys. Commun. **220**, 319 (2017).

[42] W. Lee, M. Kim, H. Jo, Y. Song, and J. Ahn, Coherent and dissipative dynamics of entangled few-body systems of Rydberg atoms, Phys. Rev. A **99**, 043404 (2019).

[43] F. Liu, Z. Yang, P. Bienias, T. Iadecola, and A. Gorshkov, Localization and criticality in antiblockaded two-dimensional Rydberg atom arrays, Phys. Rev. Lett. **128**, 013603 (2022).

[44] S. Su, E. Liang, S. Zhang, J. Wen, L. Sun, Z. Jin, and A. Zhu, One-step implementation of the Rydberg-Rydberg-interaction gate, Phys. Rev. A **93**, 012306 (2016).

[45] M. Goerz, E. Halperin, J. Aytac, C. Koch, and K. Whaley, Robustness of high-fidelity Rydberg gates with single-site addressability, Phys. Rev. A **90**, 032329 (2014).

[46] K. McDonnell, L. Keary, and J. Pritchard, Demonstration of a quantum gate using electromagnetically induced transparency, Phys. Rev. Lett. **129**, 200501 (2022).

[47] M. Mohan, R. de Keijzer, and S. Kokkelmans, Robust control and optimal Rydberg states for neutral atom two-qubit gates, Phys. Rev. Res. **5**, 033052 (2023).

[48] X. Jiang, J. Scott, M. Friesen, and M. Saffman, Sensitivity of quantum gate fidelity to laser phase and intensity noise, Phys. Rev. A **107**, 042611 (2023).

[49] R. Li, J. Qian, and W. Zhang, Proposal for practical Rydberg quantum gates using a native two-photon excitation, Quantum Sci. Technol. **8**, 035032 (2023).

[50] S. Jandura, J. Thompson, and G. Pupillo, Optimizing Rydberg gates for logical-qubit performance, PRX Quantum **4**, 020336 (2023).

[51] E. Braaten, H. Hammer, and G. Lepage, Lindblad equation for the inelastic loss of ultracold atoms, Phys. Rev. A **95**, 012708 (2017).

[52] L. Theis, F. Motzoi, F. Wilhelm, and M. Saffman, High-fidelity Rydberg-blockade entangling gate using shaped, analytic pulses, Phys. Rev. A **94**, 032306 (2016).

[53] J. Wu, S. Su, Y. Wang, J. Song, Y. Xia, and Y. Jiang, Effective Rabi dynamics of Rydberg atoms and robust high-fidelity quantum gates with a resonant amplitude-modulation field, Opt. Lett. **45**, 1200 (2020).

[54] Z. Fu, P. Xu, Y. Sun, Y. Liu, X. He, X. Li, M. Liu, R. Li, J. Wang, L. Liu, and M. Zhan, High-fidelity entanglement of neutral atoms via a Rydberg-mediated single-modulated-pulse controlled-phase gate, Phys. Rev. A **105**, 042430 (2022).

[55] S. Evered, D. Bluvstein, M. Kalinowski, S. Ebadi, T. Manovitz, H. Zhou, S. Li, A. Geim, T. Wang, N. Maskara *et al.*, High-fidelity parallel entangling gates on a neutral atom quantum computer, Nature (London) **622**, 268 (2023).

[56] X. Li, X. Shao, and W. Li, Single temporal-pulse-modulated parameterized controlled-phase gate for Rydberg atoms, Phys. Rev. Appl. **18**, 044042 (2022).

[57] M. Reetz-Lamour, T. Amthor, J. Deiglmayr, and M. Weidemüller, Rabi oscillations and excitation trapping in the coherent excitation of a mesoscopic frozen Rydberg gas, Phys. Rev. Lett. **100**, 253001 (2008).

[58] J. Thompson, T. Tiecke, A. Zibrov, V. Vuletić, and M. Lukin, Coherence and Raman sideband cooling of a single atom in an optical tweezer, Phys. Rev. Lett. **110**, 133001 (2013).

[59] L. Isenhower, E. Urban, X. L. Zhang, A. Gill, T. Henage, T. Johnson, T. Walker, and M. Saffman, Demonstration of a neutral atom controlled-NOT quantum gate, Phys. Rev. Lett. **104**, 010503 (2010).

[60] T. Wilk, A. Gaëtan, C. Evellin, J. Wolters, Y. Miroshnychenko, P. Grangier, and A. Browaeys, Entanglement of two individual neutral atoms using Rydberg blockade, Phys. Rev. Lett. **104**, 010502 (2010).

[61] D. D. B. Rao and K. Mølmer, Robust Rydberg-interaction gates with adiabatic passage, Phys. Rev. A **89**, 030301(R) (2014).

[62] I. Beterov, M. Saffman, E. Yakshina, D. Tretyakov, V. Entin, S. Bergamini, E. Kuznetsova, and I. Ryabtsev, Two-qubit gates using adiabatic passage of the Stark-tuned Förster resonances in Rydberg atoms, Phys. Rev. A **94**, 062307 (2016).

[63] D. Petrosyan, F. Motzoi, M. Saffman, and K. Mølmer, High-fidelity Rydberg quantum gate via a two-atom dark state, Phys. Rev. A **96**, 042306 (2017).

[64] X. Huang, Z. Ding, C. Hu, L. Shen, W. Li, H. Wu, and S. Zheng, Robust Rydberg gate via Landau-Zener control of Förster resonance, Phys. Rev. A **98**, 052324 (2018).

[65] I. Beterov, G. Hamzina, E. Yakshina, D. Tretyakov, V. Entin, and I. Ryabtsev, Adiabatic passage of radio-frequency-assisted Förster resonances in Rydberg atoms for two-qubit gates and the generation of Bell states, Phys. Rev. A **97**, 032701 (2018).

[66] M. Saffman, I. Beterov, A. Dalal, E. Páez, and B. Sanders, Symmetric Rydberg controlled-Z gates with adiabatic pulses, Phys. Rev. A **101**, 062309 (2020).

[67] A. Mitra, M. J. Martin, G. W. Biedermann, A. M. Marino, P. M. Poggi, and I. H. Deutsch, Robust Mølmer-Sørensen gate for neutral atoms using rapid adiabatic Rydberg dressing, Phys. Rev. A **101**, 030301(R) (2020).

[68] N. Hutzler, L. Liu, Y. Yu, and K. Ni, Eliminating light shifts for single atom trapping, New J. Phys. **19**, 023007 (2017).

[69] A. Cesa and J. Martin, Two-qubit entangling gates between distant atomic qubits in a lattice, Phys. Rev. A **95**, 052330 (2017).

[70] X. Shi and Y. Lu, Quantum gates with weak van der Waals interactions of neutral Rydberg atoms, Phys. Rev. A **104**, 012615 (2021).

[71] A. Kaufman and K. Ni, Quantum science with optical tweezer arrays of ultracold atoms and molecules, Nat. Phys. **17**, 1324 (2021).

[72] M. Marcuzzi, J. Minář, D. Barredo, S. de Léséleuc, H. Labuhn, T. Lahaye, A. Browaeys, E. Levi, and I. Lesanovsky, Facilitation dynamics and localization phenomena in Rydberg lattice gases with position disorder, Phys. Rev. Lett. **118**, 063606 (2017).

[73] Y. Yu, N. Hutzler, J. Zhang, L. Liu, J. Hood, T. Rosenband, and K. Ni, Motional-ground-state cooling outside the Lamb-Dicke regime, Phys. Rev. A **97**, 063423 (2018).

[74] X. Shao, T. Zheng, C. Oh, and S. Zhang, One-step achievement of robust multipartite Greenberger–Horne–Zeilinger state and controlled-phase gate via Rydberg interaction, J. Opt. Soc. Am. B **31**, 827 (2014).

[75] S. Su and W. Li, Dipole-dipole-interaction–driven antiblockade of two Rydberg atoms, Phys. Rev. A **104**, 033716 (2021).

[76] T. Graham, M. Kwon, B. Grinkemeyer, Z. Marra, X. Jiang, M. Lichtman, Y. Sun, M. Ebert, and M. Saffman, Rydberg-mediated entanglement in a two-dimensional neutral atom qubit array, Phys. Rev. Lett. **123**, 230501 (2019).

[77] X. Zhang, A. Gill, L. Isenhower, T. Walker, and M. Saffman, Fidelity of a Rydberg-blockade quantum gate from simulated quantum process tomography, Phys. Rev. A **85**, 042310 (2012).

[78] Y. Sun, P. Xu, P. Chen, and L. Liu, Controlled phase gate protocol for neutral atoms via off-resonant modulated driving, Phys. Rev. Appl. **13**, 024059 (2020).

[79] G. Di Domenico, S. Schilt, and P. Thomann, Simple approach to the relation between laser frequency noise and laser line shape, Appl. Opt. **49**, 4801 (2010).

[80] H. Levine, A. Keesling, A. Omran, H. Bernien, S. Schwartz, A. Zibrov, M. Endres, M. Greiner, V. Vuletić, and M. Lukin, High-fidelity control and entanglement of Rydberg-atom qubits, Phys. Rev. Lett. **121**, 123603 (2018).

[81] I. Madjarov, J. Covey, A. Shaw, J. Choi, A. Kale, A. Cooper, H. Pichler, V. Schkolnik, J. Williams, and M. Endres, High-fidelity entanglement and detection of alkaline-earth Rydberg atoms, Nat. Phys. **16**, 857 (2020).

[82] Y. Liu, Y. Sun, Z. Fu, P. Xu, X. Wang, X. He, J. Wang, and M. Zhan, Infidelity induced by ground-Rydberg decoherence of the control qubit in a two-qubit Rydberg-blockade gate, Phys. Rev. Appl. **15**, 054020 (2021).

[83] H. Tamura, T. Yamakoshi, and K. Nakagawa, Analysis of coherent dynamics of a Rydberg-atom quantum simulator, Phys. Rev. A **101**, 043421 (2020).

[84] T. Johnson, E. Urban, T. Henage, L. Isenhower, D. Yavuz, T. Walker, and M. Saffman, Rabi oscillations between ground and Rydberg states with dipole-dipole atomic interactions, Phys. Rev. Lett. **100**, 113003 (2008).

[85] D. Jaksch, J. Cirac, P. Zoller, S. Rolston, R. Côté, and M. Lukin, Fast quantum gates for neutral atoms, Phys. Rev. Lett. **85**, 2208 (2000).

[86] M. Lukin, M. Fleischhauer, R. Cote, L. Duan, D. Jaksch, J. Cirac, and P. Zoller, Dipole blockade and quantum information processing in mesoscopic atomic ensembles, Phys. Rev. Lett. **87**, 037901 (2001).

[87] E. Urban, T. Johnson, T. Henage, L. Isenhower, D. Yavuz, T. Walker, and M. Saffman, Observation of Rydberg blockade between two atoms, Nat. Phys. **5**, 110 (2009).

[88] A. Gaëtan, Y. Miroshnychenko, T. Wilk, A. Chotia, M. Viteau, D. Comparat, P. Pillet, A. Browaeys, and P. Grangier, Observation of collective excitation of two individual atoms in the Rydberg blockade regime, Nat. Phys. **5**, 115 (2009).

[89] Y. Zeng, P. Xu, X. He, Y. Liu, M. Liu, J. Wang, D. Papoular, G. Shlyapnikov, and M. Zhan, Entangling two individual atoms of different isotopes via Rydberg blockade, Phys. Rev. Lett. **119**, 160502 (2017).

[90] S.-L. Su, Y. Gao, E. Liang, and S. Zhang, Fast Rydberg antiblockade regime and its applications in quantum logic gates, Phys. Rev. A **95**, 022319 (2017).

[91] T. Weber, M. Höning, T. Niederprüm, T. Manthey, O. Thomas, V. Guarrera, M. Fleischhauer, G. Barontini, and H. Ott, Mesoscopic Rydberg-blockaded ensembles in the superatom regime and beyond, Nat. Phys. **11**, 157 (2015).

[92] D. Yu, H. Wang, J. Liu, S. Su, J. Qian, and W. Zhang, Multiqubit Toffoli gates and optimal geometry with Rydberg atoms, Phys. Rev. Appl. **18**, 034072 (2022).

[93] Y. Kang, J. Song, and Y. Xia, Error-resistant nonadiabatic binomial-code geometric quantum computation using reverse engineering, Opt. Lett. **47**, 4099 (2022).

[94] Y. Kang, Y. Xiao, Z. Shi, Y. Wang, J. Yang, J. Song, and Y. Xia, Effective implementation of nonadiabatic geometric quantum gates of cat-state qubits using an auxiliary qutrit, New J. Phys. **25**, 033029 (2023).

[95] P. Xu, Q. Jing, P. Zhao, and Y. Yu, Microwave-driven *i*SWAP-like gate for fixed-frequency superconducting transmon qutrits, Phys. Rev. A **108**, 032615 (2023).

[96] O. Gamel and D. James, Time-averaged quantum dynamics and the validity of the effective Hamiltonian model, Phys. Rev. A **82**, 052106 (2010).

[97] D. James, Quantum computation with hot and cold ions: An assessment of proposed schemes, Fortschr. Phys. **48**, 823 (2010).

[98] S. Jandura and G. Pupillo, Time-optimal two- and three-qubit gates for Rydberg atoms, Quantum **6**, 712 (2022).